

b-initiated processes at the LHC: a reappraisal

Fabio Maltoni,^a Giovanni Ridolfi,^b Maria Ubiali^c

^a*Centre for Cosmology, Particle Physics and Phenomenology CP3, Université Catholique de Louvain, Chemin du Cyclotron, 1348 Louvain-la-Neuve, Belgium*

^b*Dipartimento di Fisica, Università di Genova & INFN, Sezione di Genova
Via Dodecaneso 33, 16146 Genova, Italy*

^c*Institut für Theoretische Teilchenphysik und Kosmologie, RWTH Aachen University,
D-52056 Aachen, Germany*

E-mail: fabio.maltoni@uclouvain.be, giovanni.ridolfi@ge.infn.it,
ubiali@physik.rwth-aachen.de

ABSTRACT: Several key processes at the LHC in the standard model and beyond that involve b quarks, such as single-top, Higgs, and weak vector boson associated production, can be described in QCD either in a 4-flavor or 5-flavor scheme. In the former, b quarks appear only in the final state and are typically considered massive. In 5-flavor schemes, calculations include b quarks in the initial state, are simpler and allow the resummation of possibly large initial state logarithms of the type $\log \frac{Q^2}{m_b^2}$ into the b parton distribution function (PDF), Q being the typical scale of the hard process. In this work we critically reconsider the rationale for using 5-flavor improved schemes at the LHC. Our motivation stems from the observation that the effects of initial state logs are rarely very large in hadron collisions: 4-flavor computations are perturbatively well behaved and a substantial agreement between predictions in the two schemes is found. We identify two distinct reasons that explain this behaviour, i.e., the resummation of the initial state logarithms into the b -PDF is relevant only at large Bjorken x and the possibly large ratios Q^2/m_b^2 's are always accompanied by universal phase space suppression factors. Our study paves the way to using both schemes for the same process so to exploit their complementary advantages for different observables, such as employing a 5-flavor scheme to accurately predict the total cross section at NNLO and the corresponding 4-flavor computation at NLO for fully exclusive studies.

KEYWORDS: heavy quarks, LHC phenomenology QCD

ARXIV EPRINT: [xxxx.xxxx](https://arxiv.org/abs/xxxx.xxxx)

Contents

1	Introduction	1
2	Heavy quark schemes: a short review	4
3	Impact of resummation	6
4	Heavy quark production in lepton-hadron collisions	9
4.1	Bottom–Antibottom production	11
5	Hadron–hadron collisions	15
5.1	Associated W and bottom production	16
5.2	Single top production	22
5.3	The general case	26
6	Conclusions	29
A	LO matrix elements for heavy quark production	31
A.1	Heavy quark production (DIS and single top)	31
A.2	Associated Wb production	35
B	Higher orders	37
C	Explicit NLO expression for \tilde{b}	42

1 Introduction

Processes involving third generation quarks play a key role in collider phenomenology. The reason is twofold: on the one hand, bottom and top quarks have a very peculiar signatures with respect to light quarks that make possible an easy flavor identification. Experimentally, bottom quarks can be efficiently identified, for instance, through displaced vertices in the detector while top quarks can be detected indirectly via their decay to bottom-quarks and a W boson. On the other hand, they bring about special theoretical attention. Being the heaviest among all quarks, they do interact most strongly with the electroweak symmetry breaking sector in the standard model (SM) and in many extensions thereof. A light Higgs boson, for example, predominantly decays into bottom-antibottom quark pairs, providing the main decay channel where the Higgs associated production mechanisms (WH, ZH, ttH) can be searched for. In addition, in models like supersymmetry, where the coupling of the Higgs to bottom quarks can be comparable to that of top quark in the SM, associated production with bottom quarks can provide the largest production

mode. Many of the searches for the Higgs and for new physics in general start from final state signatures which include bottom quarks. The need for accurate theoretical predictions for such processes, both signal and backgrounds, is therefore very well motivated.

Calculations of high-energy processes involving the production of bottom quarks (and heavy quarks in general) are typically performed in two different ways. One option (which, for simplicity, will be referred to as the "massive" or 4-flavor (4F) scheme in the following) is the most straightforward from the conceptual point of view: bottom quarks are significantly heavier than the proton and therefore can be only created in pairs (or singly in association with a top quark, in the case of weak interactions) in high- Q^2 interactions. In this approach, the heavy quark does not contribute to the proton wave-function, and can only be generated as a massive final state, where the heavy quark mass can act as an infrared cut-off for the more inclusive observables. More technically, for this approach to be reliable, one assumes the heavy quark mass to be of the same order as the other hard scales involved in the process. At the same time, b -parton distribution functions are set to zero. In practice, the massive scheme amounts to employ an effective theory with n_l light quarks, where the heavy quarks are decoupled and do not enter in the computation of the running coupling constant and in the evolution of the PDFs. There are many (differential) calculations available at NLO in QCD performed in this scheme relevant for hadron collider phenomenology, including among the most important ones, $pp \rightarrow bb + X$ [1, 2], $pp \rightarrow 4b + X$ [3], $pp \rightarrow tbb + X$ [4, 5], $pp \rightarrow tbj + X$ [6], $pp \rightarrow H^\pm tb + X$ [7], $pp \rightarrow \phi bb + X$ with $\phi = H, A$ [8–11], and $pp \rightarrow Vbb + X$ with $V = W, Z$ [12–18]. However, no prediction at NNLO in QCD for any process of relevance at the LHC is available in this scheme to date.

Alternatively, one may face a situation where the typical scale Q of the process, such as the p_T of the bottom quark itself or the mass weak boson in the final state, is way higher than the mass of the heavy quark and logarithms of the type $\log \frac{Q^2}{m_b^2}$ (which can be of initial or final state nature) appear that might spoil the convergence of a fixed-order perturbative expansion. In this case, it is natural to consider a scheme where heavy quark mass are considered as small parameters, power corrections of the type $(m_b^2/Q^2)^n$ are pushed to higher orders and towers of $\log^m \frac{Q^2}{m_b^2}$ appearing at all orders explicitly resummed via usual Altarelli-Parisi evolution equations. We dub this class of approaches and their systematic improvements as "massless" or 5-flavor (5F) schemes.¹ In so doing, initial-state large logarithms are resummed into a b distribution function and final-state ones into perturbative fragmentation functions. In fact initial- and final-state logarithms have a very different status, the latter being not only better understood but also possibly avoided by introducing more inclusive observables than those related to B -mesons, such as b -jets [19] or even bb -jets [20] which are not affected in the first place by such large logs. Different is the case for initial state b 's, on which we focus in this work. Many are the (differential) NLO calculations available in this scheme too that are relevant at LHC: $pp \rightarrow tj + X$ [21–

¹We draw the reader's attention to the fact that the naming "massive" and "massless" is conventional and *it does not* imply anything on whether power-like bottom mass effects are included or not in actual calculations. There are many accurate predictions available performed in the massive scheme which do not include mass effects because they are small for the observables of interest. On the other hand, in massless "improved" schemes mass effects are normally taken into account when higher-order terms are included.

26] $pp \rightarrow tW + X$ [24, 27], $pp \rightarrow H^\pm t + X$ [28, 29] $pp \rightarrow \phi(bb) + X$ [30], $pp \rightarrow \phi b(b) + X$ with $\phi = H, A$ [31], $pp \rightarrow Vb + X$ [32, 33], and $pp \rightarrow Vbj + X$ [34, 35] with $V = W, Z$. In addition, $pp \rightarrow \phi(bb) + X$ with $\phi = H, A$ [36] and $pp \rightarrow Z(bb) + X$ [37] are also available at NNLO.

Both schemes present advantages and disadvantages and are typically adopted in complementary regimes depending on the relative size of the heavy quark masses relative to the scale Q of the process. It turns out that in the massless schemes calculations are highly simplified: in the Born configuration the number of external legs as well as the scales in the processes are reduced. Mass and “spectator heavy quarks” effects appear at higher orders and can be systematically added. In addition, as mentioned above, potentially large logarithms of the ratio Q^2/m_b^2 arising from collinear splitting of the initial heavy quarks and gluons, are consistently resummed in the heavy quark PDF. In the massive scheme instead, the computation is more complicated due to the presence of massive final states and higher multiplicity; however, the full kinematics of the heavy quarks is taken into account already at the leading order and can be accurately studied via a next-to-leading order computation. In the latter case, the implementation in parton shower codes is also straightforward as no complications due to the inherent arbitrariness in the description of massive effects arise. The downside is that possibly large logarithms developing in the initial (and also the final state) are not resummed and could lead to a poorly-behaved perturbative expansion. In this work we will argue that in fact, at hadron collider, this is hardly the case for a large class of processes/observables, and such resummation effects are quite mild in general and often smaller than other approximations inherent in fixed order calculations.

To all orders in perturbation theory the two schemes can be defined such as to be exactly identical. On the other hand, the way of ordering the perturbative expansion is different and at any finite order the results might not necessarily match. This is the case for the many 5F improved schemes available which typically differ order-by-order in perturbation theory due to the different possible choices in including subleading terms. For some processes the difference between leading order calculations performed in the two schemes may be very significant and in extreme cases have yielded to (only apparently) puzzling predictions differing up to an order of magnitude as in the case of the b -initiated Higgs production [9, 30, 31, 37–39].

In this work we critically reconsider the motivations for using 5F or massless improved schemes in which potentially large logarithms are resummed. Our aim *is not* to analyse in detail the technical differences between the various approaches to 5F improved schemes, but to assess the relevance of the large logarithms in first place for processes of interest to LHC phenomenology and the need or not to employ such schemes. Our argument is based on two main points. First on a simple yet quantitative study of the importance of the resummation effects in b distribution functions with respect to having only explicit leading and subleading logs at fixed order. Second on the systematic assessment of the size of such logs in 4F calculations. To this aim, we perform a thorough analysis of their origin and role in various processes initiated by a single bottom. We analyse in detail some representative processes that can be treated analytically and cover a broad spectrum of possibilities. In

the single heavy quark category fall both lepton-hadron (e.g. DIS) and hadron-hadron collider processes. The first category is mostly interesting for pedagogical reasons, and because it is the place where heavy flavor schemes have been profusely discussed in the literature. It might also be interesting in view of the LHeC electron proton collider [40]. In the hadron-hadron processes we consider both $2 \rightarrow 2$ processes like associate bottom and vector boson production and $2 \rightarrow 3$ processes like single top production.

As a result, we will argue that at the LHC, the logs that are resummed in b distribution functions, apart from extreme cases which we will clearly identify, are not very large because the possibly large ratios Q^2/m_b^2 's are always accompanied by universal phase space suppression factors at all orders in perturbation theory. Such logs, therefore, do not spoil the convergence of the perturbative series of the 4F flavor scheme whose results are in general well-behaved. 5F schemes calculations, on the other hand, do typically display smaller scale uncertainties leading to more accurate predictions for very inclusive observables, such as total rates. However, for differential distributions and more exclusive observables their predictions might be less accurate, technically more involved and in general less suitable to theoretical-experimental comparisons with respect to those performed via NLO computations in the 4F scheme interfaced to parton showers, employing MC@NLO [41] or the POWHEG [42] methods.

The paper is organized as follows. In Section 2 we provide a brief overview on the various possibilities available in the literature for the implementing 5F (improved) schemes. The section is meant for a reader who is not familiar with the subject and would like to learn the basic concepts/techniques as well as where to find more details in selected references. In Section 3 we show that, apart from extreme kinematical situations, the resummation effects in the b -distribution functions are mild compared to the contributions from the explicit leading and subleading logs present at fixed order in 4F scheme calculations. In Section 4 the DIS case is discussed. This allows to set the stage and illustrate our analysis approach in a simple and very instructive case, where $\log \frac{Q^2}{m_b^2}$ are clearly identified and whose relevance can be easily studied as a function of the kinematical setup. In Section 5 we finally attack processes at the LHC and show that initial collinear logarithms are typically not very large. The last section presents a summary together with our conclusions.

2 Heavy quark schemes: a short review

Processes involving heavy quarks often provide a good example of multi-scale processes. First, let us define a heavy quark to be one whose mass m is large enough that the effective coupling at the scale of a heavy quark mass $\alpha_s(m^2)$ is in the perturbative region. With this definition, the bottom and top quarks are definitely heavy quarks. The charm quark mass, on the other hand, is rather close to the boundary region and QCD perturbative corrections at the scale of the charm mass are generally large, and can only be taken as an indication.

Whenever a cross section is characterised by two different scales, here the hard scale Q and the mass of a heavy quark m , perturbative calculations typically display both logarithms and powers of the ratio m^2/Q^2 . The former contributions may spoil the accuracy

of the calculation if $Q \gg m$. It is easy to trace back the dynamical origin of such logs to the process of gluon splitting into a heavy quark-antiquark pair. Such splitting can take place either in the initial or in the final state. As already mentioned, final state logs can be resummed into fragmentation functions or cancelled by defining more inclusive observables such as heavy-quark jets [19]. In the following, we focus on the logarithms arising from initial state gluon splitting. By defining a heavy quark parton density, one would automatically resum the logarithms to all orders in perturbative QCD via the Dokshitzer-Gribov-Lipatov-Altarelli-Parisi (DGLAP) evolution equations: when computing the heavy quark parton densities from the 1-loop DGLAP evolution equations, all possible multiple collinear gluon emission from the initial state are in effect summed up to all orders in α_s in the leading-log approximation. However, this approach is only adequate at large Q , where the mass of the heavy quark is small with respect to the typical scale of the process. At smaller Q , powers of $\log(Q^2/m^2)$ do not spoil perturbation theory, and power corrections m^2/Q^2 need to be consistently included.

Theoretical predictions in QCD have been performed according to a variety of schemes for dealing with heavy quark masses. We restrict our discussion to two (classes of) schemes for dealing with the b distribution, which we denote by 5F or massless and 4F or massive schemes. Technically, our definition of the 4F scheme corresponds to the so-called Fixed Flavor Number (FFN) scheme with $n_f = 4$. In this scheme the bottom quark appears only among the final state particles, and is not associated to a PDF. Calculations in the 4F scheme are meant to provide reliable results when the scale of the process is not much larger than m . At any finite order in a perturbative calculation, the FFN result is expected to break down as the scale becomes large compared to m .

Natural extensions of the FFN scheme are the so-called Variable Flavor Number (VFN) schemes, which consist of a sequence of n_f -flavor FFN, each in its region of validity, consistently matched at the transition thresholds. There are, however, several ways of implementing a VFN scheme. The simplest implementation of the VFN scheme is the zero-mass (ZM) approximation, where all quarks are treated as massless. Heavy quarks are absent at scales $\mu^2 < m^2$, and they are radiatively generated at the transition points $\mu^2 = m^2$ by the subprocess $g \rightarrow Q\bar{Q}$, but apart from this they are treated as massless partons. The ZM-VFN scheme is therefore a combination of massless $\overline{\text{MS}}$ schemes characterized by different numbers of light flavors n_l . Basically the only mass effects are due to the change of number of flavors in the QCD β function and in the anomalous dimensions as one crosses the heavy quark thresholds. The coefficient functions are calculated under the assumption that all active partons are massless, with the associated singularities subtracted in the $\overline{\text{MS}}$ scheme. This scheme becomes inaccurate for scales close to the thresholds. This does not depend uniquely on the fact that $\mathcal{O}(m^2/Q^2)$ terms are neglected in the coefficient functions, but also on the approximate treatment of the phase space and the arbitrariness in the definition of the scaling variable, i.e. the fraction of energy in the collision taken by the heavy quark. Due to the absence of mass effects, the ZM formalism is not a good approximation in the region near the physical thresholds.

In the following, with 5F we indicate a scheme where the collinear logarithms appearing in each term of the FFN scheme computation are resummed to all orders in the heavy quark

PDF, and where powers of m^2/Q^2 are consistently included at higher orders. These schemes are called General–Mass VFN scheme and all partons, including the bottom, are associated to a parton distribution function above threshold. The GM-VFN scheme represents an improvement over the ZM-VFN scheme. However, it also introduces new ambiguities with respect to the shifting of higher-order terms into the lower-order expressions. In the GM-VFN schemes the mass of the heavy quarks is taken into account in the partonic cross sections, and the schemes are designed to interpolate between the FFN scheme, which gives a correct description of the threshold region, and ZM-VFNS which accounts for large energy logarithms. The first proposed matching technique for the inclusion of mass-suppressed contributions, built upon the CWZ renormalization scheme [43], was developed long ago; it is the so-called ACOT scheme [44]. It provides a mechanism to incorporate the heavy quark masses in theoretical calculations both kinematically and dynamically. It yields the complete quark mass dependence from the low to high energy regimes; for $m \gg Q$ it ensures manifest decoupling, and in the limit $m \ll Q$ it reduces precisely to the $\overline{\text{MS}}$ scheme without any finite renormalization term. Several variants of this method were subsequently proposed, such as S-ACOT [45] or ACOT- χ [46], which include some improvements and/or simplifications with respect the original ACOT scheme. A different approach, the Thorne-Roberts [47] VFN scheme or TR' [48] in its latest version, emphasizes the correct threshold behaviour and includes higher-order terms in order to smoothen the function at the transition points. Namely, the NLO computation includes $\mathcal{O}(\alpha_s^2)$ terms, which formally belong to the next-to-next-to-leading order, which are introduced in order to cure the discontinuities of the physical observables at the heavy quark mass threshold. An alternative approach considers both massless and massive scheme calculations as power expansions in the strong coupling constant, and replaces the coefficient of the expansion in the former with their exact massive counterpart in the latter. A first step in this direction was taken in Ref. [49]. More recently, another method, called FONLL, was introduced in Ref. [50] in the context of hadroproduction of heavy quarks, and was recently applied to deep-inelastic structure functions in Ref. [51]. Most of the up-to-date parton sets [52–56] implement one of the above mentioned matched scheme as a default scheme. On top of that, each collaboration also provides FFNS parton sets with $n_f = 3, 4, 5$. Other PDF fitting collaborations [57, 58] provide as default sets FFNS parton sets with $n_f = 3, 4, 5$. At a fixed order n in perturbation theory, the difference between these schemes amounts to adding different $\mathcal{O}(\alpha_s^{n+1})$ higher-order terms, therefore the difference is reduced as one increases the perturbative order. A benchmark comparison is available in Ref. [59].

3 Impact of resummation

In the previous section we have distinguished the 4F schemes, where b -PDFs are not present and collinear logarithms of the mass of the bottom are not resummed, and the 5F schemes, where instead this class of logarithms is resummed. The question we address in this section is the following:

- What is the typical size of the effects of the resummation of initial state collinear logs

of the type $\log \mathcal{Q}^2/m_b^2$ with respect to an approximation where only logs at a finite order in perturbation theory are kept?

While a detailed answer clearly depends on the kinematic regime considered, it is interesting to explore the possibility that general features might be present at colliders in general and at the LHC in particular. Quite surprisingly, while already addressed in the past in several specific contexts, to our knowledge it has never been answered for b -PDF's.

In order to assess the relevance of the resummation of logarithms of \mathcal{Q}^2/m^2 performed in the 5F scheme, one must compare the exact solution of DGLAP equations, and its expansion in powers of α_s up to a given fixed order. This comparison can be easily performed analytically at leading order. In this case the full b parton density is a solution of the evolution equation (in Mellin moment space)

$$\frac{d}{d \log \mu^2} b(N, \mu^2) = \frac{\alpha_s(\mu^2)}{2\pi} \left[\gamma_{qq}^{(0)}(N) b(N, \mu^2) + \gamma_{qg}^{(0)}(N) g(N, \mu^2) \right], \quad (3.1)$$

where $g(N, \mu^2)$ is the Mellin-transformed gluon distribution, $\gamma_{ij}^{(0)}$ are the leading order Altarelli-Parisi anomalous dimensions, and the initial condition is $b(N, m_b^2) = 0$. This equation can be easily solved if the gluon scale dependence is neglected, an approximation which is valid at this order if N (i.e., x) is not too small. A straightforward calculation yields

$$b(N, \mu^2) = \frac{\gamma_{qg}^{(0)}(N)}{\gamma_{qq}^{(0)}(N)} \left\{ \left[1 + \frac{\alpha_s(m_b^2)}{2\pi} \beta_0 \log \frac{\mu^2}{m_b^2} \right]^{\frac{\gamma_{qg}^{(0)}(N)}{\beta_0}} - 1 \right\} g(N, m_b^2), \quad (3.2)$$

where $\beta_0 = 11 - \frac{2}{3}n_f$. This solution can be expanded in powers of $\alpha_s(m_b^2)$. Using the binomial expansion

$$(1+x)^a = \sum_{k=0}^{\infty} \frac{\Gamma(a+1)}{\Gamma(a-k+1)} \frac{x^k}{k!} \quad (3.3)$$

and standard properties of the Γ function we find

$$b(N, \mu^2) = \gamma_{qg}^{(0)}(N) g(N, m_b^2) \left\{ \frac{\alpha_s(m_b^2)}{2\pi} \log \frac{\mu^2}{m_b^2} + \sum_{k=2}^{\infty} A_k(N) \frac{1}{k!} \left[\frac{\alpha_s(m_b^2)}{2\pi} \log \frac{\mu^2}{m_b^2} \right]^k \right\}, \quad (3.4)$$

where

$$A_k(N) = \left[\gamma_{qq}^{(0)}(N) - \beta_0 \right] \left[\gamma_{qq}^{(0)}(N) - 2\beta_0 \right] \dots \left[\gamma_{qq}^{(0)}(N) - (k-1)\beta_0 \right]. \quad (3.5)$$

Clearly, the resummation terms of order α_s^2 and higher become relevant when the factorization scale μ , typically of the order of the hard scale \mathcal{Q} of the process, is much larger than m_b . We note, however, that the coefficients $A_k(N)$ behave as $\log^k N$ at large N , due to the large- N behavior $|\gamma_{qq}^{(0)}| \sim \log N$, originated by the soft pole in the Altarelli-Parisi splitting function. We therefore expect the effects of resummation to be more important as the momentum fraction z gets close to 1, which corresponds to the large- N region in Mellin space.

As we will see in the following, this simple derivation nicely reproduces the qualitative behaviour of the evolution of the b -PDF at medium to large x both at LO and NLO. However, the approximation of no-evolution for the gluon pdf is untenable at small x and therefore it cannot be used in this regime. In fact, as we will show in the following, even the exact evolution at LO is not reliable at small x and the NLO accuracy is needed.

If no intrinsic bottom content of the proton is envisaged, then the bottom parton density which appears in the 5F scheme is generated at threshold (by setting $b(x, m_b^2) = 0$ as a boundary condition) by gluon and light parton distributions. As a result the bottom PDF is not an independent quantity: it depends on the four-light flavour (u, d, c, s) and the gluon (g) densities in the 4F scheme. Following the notation of Ref. [49] the bottom PDF can be written as a function of the light flavor singlet and the gluon up to $\mathcal{O}(\alpha_s^2)$ as

$$\begin{aligned} b^{(p)}(x, \mu^2) &\equiv \tilde{b}^{(p)}(x, \mu^2) + \mathcal{O}(\alpha_s^{p+1}(\mu)) \\ &= \sum_{i=q,g} \int_x^1 \frac{dz}{z} f_i^{4F,(p)}\left(\frac{x}{z}, \mu^2\right) A_{i,b}^{(p)}\left(z, \frac{\mu^2}{m_b^2}\right), \end{aligned} \quad (3.6)$$

where by $\tilde{b}^{(p)}$ we indicate the approximated b distribution that one obtains when truncating the perturbative expansion of the bottom PDF evolution at $\mathcal{O}(\alpha_s^p)$. The operator matrix elements $A_{i,k}^{(p)}$ have been computed in the Mellin N -space in the asymptotic limit $Q^2 \gg m_b^2$ up to $\mathcal{O}(\alpha_s^3)$ and in the physical x -space up to $\mathcal{O}(\alpha_s^2)$ in Refs. [49, 60–65]. In the physical x -space up to $\mathcal{O}(\alpha_s^2)$, they read

$$\begin{aligned} \tilde{b}^{(2)}(x, \mu^2) &= \int_x^1 \frac{dz}{z} \Sigma^{4F,(2)}\left(\frac{x}{z}, \mu^2\right) \left(\frac{\alpha_s}{4\pi}\right)^2 a_{\Sigma,b}^{(2)}(z, \mu^2/m_b^2) \\ &+ \int_x^1 \frac{dz}{z} g^{4F,(2)}\left(\frac{x}{z}, \mu^2\right) \left[\left(\frac{\alpha_s}{4\pi}\right) a_{g,b}^{(1)}(z, \mu^2/m_b^2) + \left(\frac{\alpha_s}{4\pi}\right)^2 a_{g,b}^{(2)}(z, \mu^2/m_b^2) \right], \end{aligned} \quad (3.7)$$

where $\Sigma = \sum_{i=1}^{n_l} (q_i + \bar{q}_i)$ and $\alpha_s \equiv \alpha_s(\mu_R^2)$. The explicit coefficients, taken from Ref. [49], are given in Appendix C. Note that in the above formula, the ⁽¹⁾ and ⁽²⁾ superscripts indicate the perturbative order for both the perturbative matching coefficient and the PDFs. At LO, it is easy to check that $\tilde{b}^{(1)}$ is the first term in Eq. (3.4), namely

$$\tilde{b}^{(1)}(x, \mu^2) = \frac{\alpha_s}{2\pi} \log \frac{\mu^2}{m_b^2} \int_x^1 \frac{dz}{z} P_{qg}(z) g\left(\frac{x}{z}, \mu^2\right). \quad (3.8)$$

In order to assess the accuracy of the $\mathcal{O}(\alpha_s^1)$ and $\mathcal{O}(\alpha_s^2)$ approximation, we plot in Fig. 1 the ratio $\tilde{b}(x_0, \mu)/b(x_0, \mu)$ as a function of μ between m_b and $10^2 \times m_b$, for several values of x_0 . Deviations from 1 of these curves are an indication of the size of terms of $\mathcal{O}(\alpha_s^2)$ ($\mathcal{O}(\alpha_s^3)$) and higher which have been resummed in the QCD evolution of the heavy quark PDFs.

We observe that at LO the higher order logarithms are important and that the $\tilde{b}^{(1)}$ approximation is up to 40% lower than the b distribution at large x . At small x , on the other hand, the ratio becomes larger than one, clearly suggesting the inadequacy of the LO approximation to perform a meaningful resummation.

The NLO ratio, displayed in the middle and bottom plots of Fig. 1, clearly shows that the explicit collinear logs present in a 4F calculation at NLO already provide a rather accurate approximation of the whole resummed result at NLL, significant effects of order up to 20% appearing predominantly at large Bjorken x . At small x , the resummation at NLO is well behaved and predicts very small differences between \tilde{b} and b . It would be interesting to explore and understand more in detail the small x evolution of the b -PDF and in particular the origin of such a large difference between LO and NLO results. While going somewhat beyond the scope of this paper, it is possible to qualitatively understand why the LO approximation appears too crude in this region. At small x , i.e. at small N , the evolution is dominated by the rightmost pole of the anomalous dimensions, which is located at $N = 1$ because of the singularity at $x = 1$ in the Altarelli-Parisi splitting functions. This singularity appears in P_{qq} and P_{qg} only at NLO (while it is present in P_{gq} and P_{gg} already at leading order), and therefore its impact is missed by leading-order evolution.

Our results are consistent with previous findings in the context of the c -PDF [49] even though for the charm PDF the effect of the resummation is more important, as it is also clearly shown in Ref. [66]. They also provide a very simple explanation to the somewhat counterintuitive fact that for b -initiated processes, such as for example single-top [67] and Hbb [68], total cross sections calculated in the 5F scheme differ with respect to the 4F ones more at the Tevatron than at the LHC. Naively, one could either expect the size of the logs to be independent of the collision centre-of-mass energy or were this not the case (as we will argue in the next section) to have more phase space available at higher energy to 'develop' large logs and therefore effects of resummation to be more important the higher the collider energy. The dependence on the Bjorken x of the resummation and in particular the larger effects present at higher x , on the contrary, do point to more important differences at small collider energies, as effectively seen.

4 Heavy quark production in lepton-hadron collisions

The production of heavy quarks in lepton-hadron scattering is one of the first processes for which the choice of the heavy flavor schemes has been extensively analysed from both the theoretical and the experimental points of view. For a broad overview see Refs. [44, 46, 49, 51, 69–75] and references therein and the experimental analyses performed by the H1 and ZEUS collaborations [76–82].

The relevant cross section can be expressed in terms of the structure functions usually defined in the context of deep-inelastic scattering. The contribution of heavy-quark final states to DIS structure functions has been historically computed in the massive scheme, where a heavy quark-antiquark pair is produced via vector boson-gluon fusion, as shown in the left diagrams of Fig. 2.

Alternatively, one can adopt a variable flavor number scheme, whose leading-order contribution is shown in the right diagram of Fig. 2. The main difference between the two production mechanisms can be attributed to the fact that for massive heavy quark production the quark and the anti-quark are produced in pairs, while in the second approach only

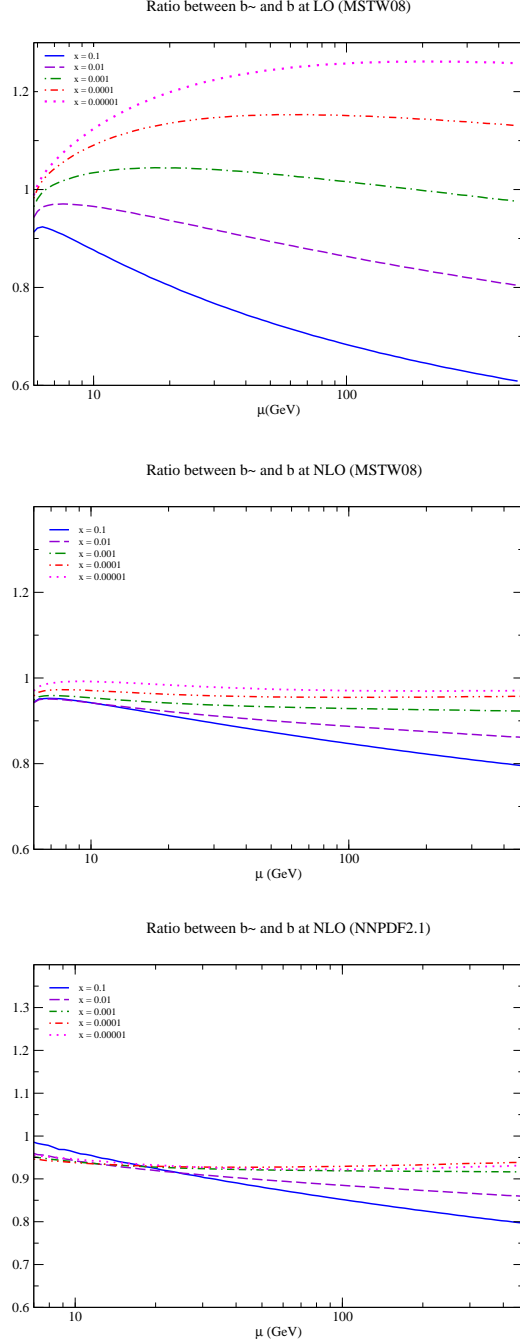


Figure 1. Ratio \tilde{b}/b for several values of x as a function of the scale μ . The 4F-FFNS and GM-VFNS are associated to the \tilde{b} and b PDF computations respectively at LO (top) and NLO order (centre and bottom) for the MSTW08 [54] and NNPDF21 [52] parton sets.

one heavy quark is produced at the leading-order. This difference reflects in the transverse momentum distribution of the bottom quark. At NLO, however, these striking differences are milder as, for instance, the gluon splitting process appears also in the massless scheme.

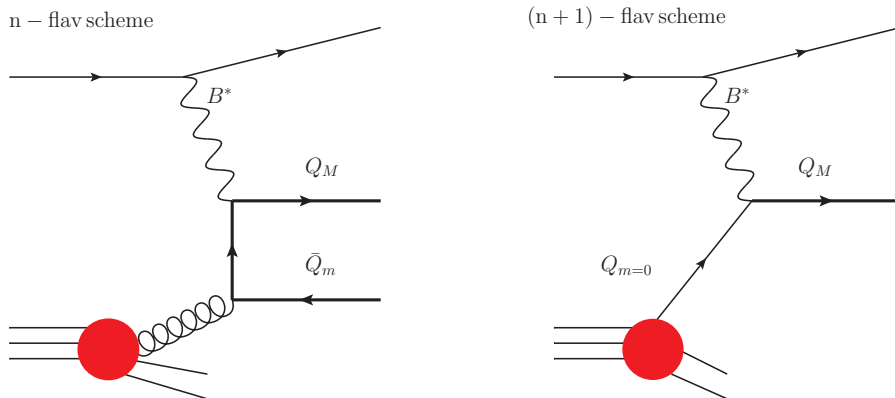


Figure 2. Leading-order diagrams for heavy quark production in a n -flavor (left) and $(n+1)$ -flavor (right) schemes.

4.1 Bottom–Antibottom production

The total cross section for the process of heavy quark production in DIS can be written

$$\sigma_b(\mu^2) = \int_{y_{\min}}^{y_{\max}} dy \int_{Q_{\min}^2}^{Q_{\max}^2} dQ^2 \frac{2\pi\alpha_l\alpha_h}{y(M^2 + Q^2)^2} \left\{ [1 + (1-y)^2]F_2^b(x, Q^2, m_b^2) - y^2 F_L^b(x, Q^2, m_b^2) + [1 - (1-y)^2]F_3^b(x, Q^2, m_b^2) \right\}, \quad (4.1)$$

where α_l, α_h are the lepton and quark coupling constants to the exchanged vector boson, M its mass, Q^2 its virtuality, and

$$y = \frac{Q^2}{xS}, \quad (4.2)$$

where S is the centre-of-mass energy squared. The functions $F_{2,L,3}^b$ are the contributions to deep-inelastic scattering structure functions coming from bottom quark production. A dependence of the total cross section on renormalization and factorization scales arises because the calculation is performed at a finite order in the QCD perturbative expansion.

We start our analysis by comparing the scale dependence of the 4F and 5F calculations. For simplicity, renormalization and factorization scales are taken to be equal. We choose

$$\mu_F = \mu_R = k\sqrt{Q^2 + 4m_b^2} \quad (4.3)$$

and we let k vary between 0.5 and 2. We have studied the scale dependence of both 4F and 5F results for two different experimental configurations: the HERA Run II and one of the possible future LHeC scenarios. At HERA the beam energies are $E_p = 920$ GeV and $E_e = 27.5$ GeV, and the kinematical cuts on the outgoing electron are set to

$$Q^2 \geq 20 \text{ GeV}^2, \quad 0.05 \leq y \leq 0.7$$

as in Ref. [81] In the LHeC scenario the energy of the proton beam has been set to $E_p = 7$

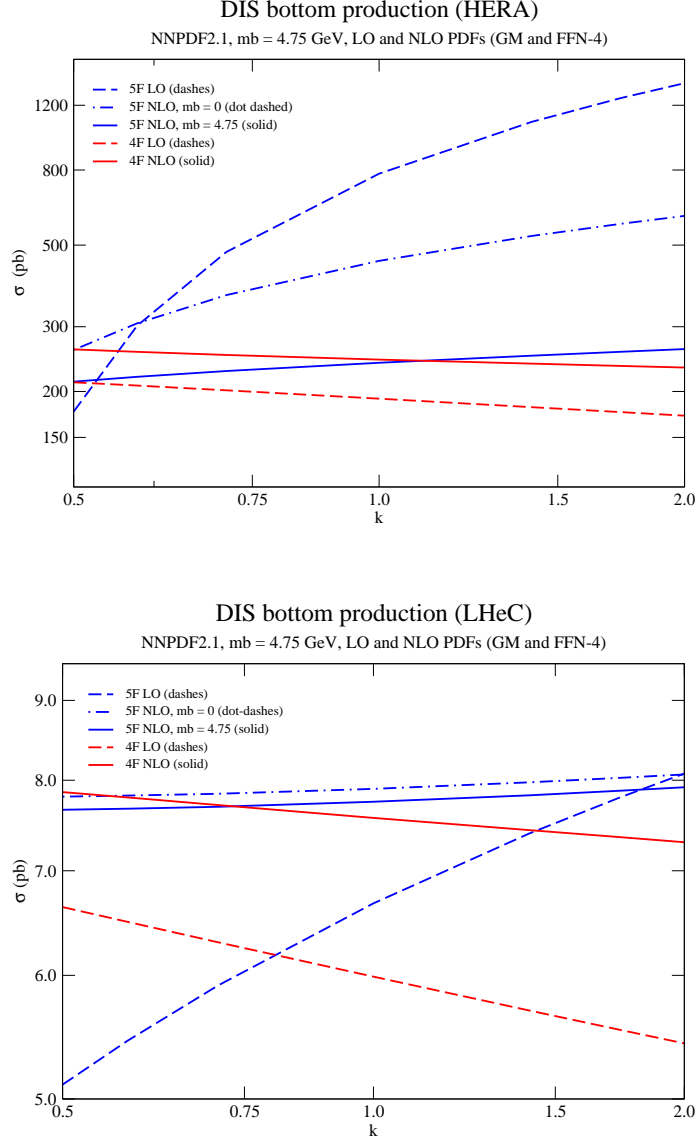


Figure 3. Comparison between 4F and 5F production for $b\bar{b}$ production at HERA run II (top) and LHeC (bottom). Input PDFs: NNPFD2.1_{FFN_NF4} (LO and NLO) for the 4F scheme (run with HVQDIS) and NNPFD2.1 (LO and NLO) for the 5F scheme (run with internal code). Parameters: $m_b = 4.75$ GeV, $k = \mu/\sqrt{Q^2 + 4m_b^2}$, with $\mu = \mu_F = \mu_R$.

TeV and that of the electron beam to $E_e = 50$ GeV. The cuts in y and Q^2 are set to

$$Q^2 \geq 2000 \text{ GeV}^2, \quad 0.1 \leq y \leq 0.9$$

The results are shown in Fig. 3. The 4F scheme curves are obtained by running the code HVQDIS [83], which is based on the calculation of Ref. [84]. The 5F curves have been computed using the results presented in Ref. [51].

In the HERA II configuration the flavor excitation (the LO $2 \rightarrow 2$ process) is considerably larger than the other predictions, being completely driven by the b quark PDF, which does not provide any transverse momentum for the produced bottom quark. At NLO, the Zero Mass prediction (where m_b is set to 0 everywhere except in the boundary conditions for the evolution of the b PDF) displays a sizeable scale dependence, even though it is milder than in the pure flavor excitation. The matched prediction, computed according to the FONLL-A scheme, where the collinear logarithms are resummed and mass effects are also taken into account, shows a mild dependence on the scale and it is close to the predictions of the 4F scheme. This indicates that, in the low Q^2 region covered in this experimental configuration, finite- m_b effects dominate over the effects due to the resummation of the logarithms, which we expect to be very small.

In the LHeC configuration, where much larger Q^2 scales are probed, the scale dependence of the 4F LO prediction displays a scale dependence which is comparable to the one of the 5F LO prediction, the former being driven by the α_s scaling and the second being driven by the bottom PDF evolution, which go in opposite directions. At NLO the ZM and the FONLL predictions in the 5F scheme are very close to each other, thereby showing that the size of finite- m_b effects are much smaller at such high scales. On the other hand, as compared to the 4F NLO prediction, they display a milder scale dependence. This tells us that in this kinematic region the resummation of the collinear logarithms dominates over the finite m_b mass effects.

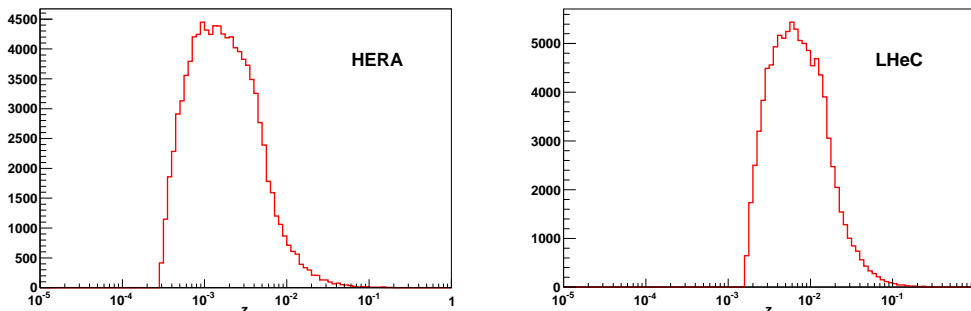


Figure 4. Distributions of events as a function of momentum fraction carried by the bottom quark in the LO 5F $eb \rightarrow eb$ process, in the HERA (left) and LHeC (right) configurations. Input PDF: NNPDF21 (LO)

In Fig. 4 we plot the distribution of the momentum fraction z carried by the bottom quark in the 5F process. We see that the distribution has a maximum at $z \sim 10^{-3}$ for the HERA II kinematics, while the peak shifts to larger values, $z \sim 10^{-2}$, in the LHeC case. Comparing to the plots in Fig. 1, we conclude that indeed at the LHeC the \tilde{b} approximation works much worse than at HERA, not only because of the larger energy scales probed in the latter kinematic region, but also because the relevant values of the parton fraction z are comparatively larger than in the case of HERA II.

We now turn to the problem of the scale choice for collinear emission. The explicit

expression of the LO partonic cross-sections for $b\bar{b}$ production in DIS is reported in Appendix A. The partonic cross-sections $d\hat{\sigma}_2$, relevant for the structure function F_2^b , displays logarithmic contributions both in the t - and u -channels, which become large as $m_b \rightarrow 0$. In order to see this explicitly, and to compare the results in the 4F and 5F schemes, it is useful to rewrite Eq. (A.16) as a Laurent expansion around $t - m_b^2 = 0$ in order to isolate the collinear singularity, and further neglect terms which are suppressed by powers of m_b^2/Q^2 . We obtain

$$\frac{d\hat{\sigma}_2}{dt} = \frac{\pi\alpha_e e_b^2 \alpha_s C_F}{16} \left[-\frac{4z}{Q^2(t - m_b^2)} \frac{z^2 + (1 - z)^2}{2} + \text{non-singular terms} \right], \quad (4.4)$$

where $z = Q^2/(s + Q^2)$. The rhs of Eq. (4.4) is immediately recognized to be proportional to the Altarelli–Parisi splitting function $P_{qg}(z)$ as reported in Eq. (C.4). The contribution of the collinear region to the cross-section takes the form dictated by the factorization theorem:

$$\begin{aligned} \int_{t_-}^{t_+} dt \frac{d\hat{\sigma}_2}{dt} &= \frac{\pi\alpha_e e_b^2 \alpha_s C_F}{4Q^2} z P_{qg}(z) \log \frac{1 + \beta}{1 - \beta} \\ &= \left(\frac{\pi^2 \alpha_e e_b^2 C_F}{2Q^2} \right) \frac{\alpha_s}{2\pi} z P_{qg}(z) \left[\log \frac{m_b^2}{s} + O\left(\frac{m_b^2}{s}\right) \right], \end{aligned} \quad (4.5)$$

where we have used

$$t_{\pm} = m_b^2 - \frac{s + Q^2}{2} (1 \pm \beta); \quad \beta = \sqrt{1 - \frac{4m_b^2}{s}}. \quad (4.6)$$

Thus, as expected, the contribution of the collinear region is proportional to

$$\frac{\alpha_s}{2\pi} P_{qg}(z) \log \frac{s}{m_b^2} = \frac{\alpha_s}{2\pi} P_{qg}(z) \log \left[\frac{Q^2}{m_b^2} \frac{1 - z}{z} \right] \quad (4.7)$$

In a leading-order 5F computation, only this logarithmically divergent contribution is taken into account, and resummed to all orders in the evolution of the b parton density. The argument of the collinear logarithm in the 5F scheme is $\frac{\mu_F^2}{m_b^2}$, and the factorization scale μ_F^2 is chosen to be Q^2 . We now note that in the full massive calculation, Eq. (4.7), the scale is not simply proportional to Q^2 , but rather to the invariant mass of the produced $b\bar{b}$ pair

$$L_{\text{DIS}} \equiv \log \left[\frac{Q^2}{m_b^2} \frac{1 - z}{z} \right] = \log \frac{M_{b\bar{b}}^2}{m_b^2}. \quad (4.8)$$

The scale of the logarithm in Eq. (4.7) is a dynamical scale which changes on an event-by-event basis depending on the momentum fraction carried by the gluon and on the kinematic invariants Q^2 and z . (This is well known for example in the context of Sudakov resummation [85], where $Q^2(1 - z)$ is identified as the characteristic energy scale of soft emission.)

Therefore, to make any consideration about its size, for a given collider energy and acceptance, one has to check what is the distribution of $(1-z)/z$. In the case this distribution is peaked in a region which is much smaller than one, then the logarithms of (M_{bb}^2/m_b^2) are not in fact large, even when $Q^2 \gg m_b^2$. If, on the other hand, it is close or even larger than one, logarithms should be resummed.

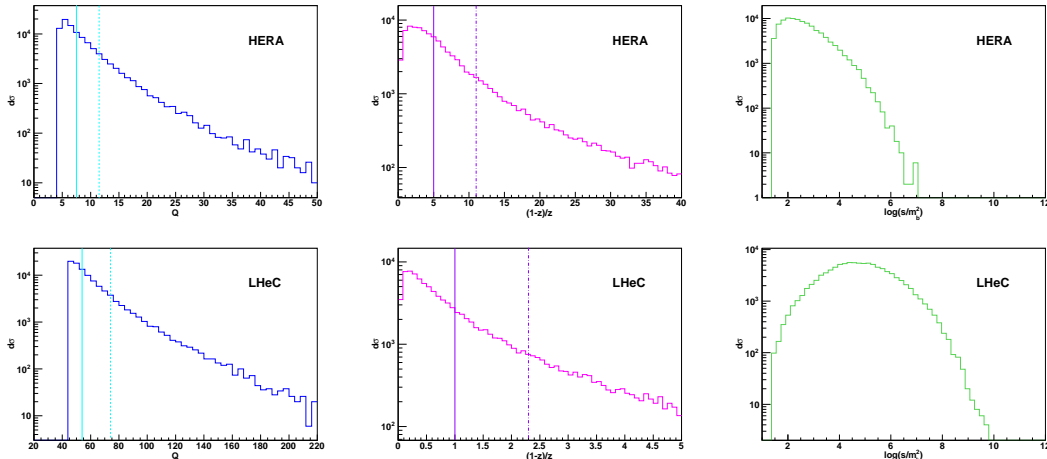


Figure 5. Distributions of events as a function of Q (left), $\frac{1-z}{z}$ (centre) and $\log(s/m_b^2)$ (right) for HERA II (top) and LHeC (bottom). In left and centre plots, 50% (80%) of events are to the left of the vertical solid (dot-dashed) line. Input PDF: NNPDF21_FFN_NF4 (LO).

In Fig. 5 we plot the distributions of Q , $\frac{1-z}{z}$ and the collinear logarithm. From the plot of the Q distribution we see that the two experimental configurations we are considering do really explore two complementary regions: for HERA II the bulk of events lies in the region $Q \gtrsim m_b$, while at LHeC Q is typically much larger than m_b . The event distribution in the kinematic factor $\frac{1-z}{z}$ is also rather different in the two cases. For HERA II, 80% of events are in the region $(1-z)/z \lesssim 10$. This means that the scale of the logarithm is sizeably larger than Q^2/m_b^2 for a large fraction of events. Therefore, even if the experimental cuts are such that Q^2 lies in a region where $\log(Q^2/m_b^2)$ is very small, the effect of these logarithms is enhanced by a scale which is effectively up to ten times larger than Q^2 . As a result, in this case the logarithms are not as negligible as one would expect from the typical size of Q^2 . On the other hand, in the LHeC kinematics the prefactor $\frac{1-z}{z}$ is peaked around a value smaller than one. This means that in the LHeC configuration the scale associated to the collinear splitting is slightly smaller than Q^2 but not dramatically and that therefore the logarithms which are resummed in the bottom PDF are significant as one would expect by looking at the Q^2 distribution.

5 Hadron–hadron collisions

In this section we discuss b -initiated processes at hadron colliders. Such processes fall in two wide categories depending whether they can be described by one or two b 's in the initial

state. Associated production of a b plus a jet, a W or Z boson, a Higgs boson, t -channel and associated tW and tH^+ single top production are examples of the first class, while Zbb and Hbb production of the second. For the sake of the argument, in this work we mainly focus on one- b initiated processes. In fact, as we will argue in the final discussion, two- b initiated processes can be analysed following the same lines providing, for instance, a useful framework to decipher well-known apparent discrepancies between 4F and 5F predictions for $pp \rightarrow Hbb$ production [68].

We will consider specifically W production initiated by a bottom quark, and single top production. The large energy scale associated to these processes is the invariant mass of the final state, rather than the high virtuality of the incoming particles, at variance with DIS. As we will prove in the following this makes a difference in the phase space available for the spectator b quark or extra radiation in general. In addition, single top provides already all the kinematical complexity needed to obtain a general expression for the initial-state collinear logarithm, a form that can then be used for any process of this type, including those involving two b 's in the initial state.

We first analyse the associated production of a heavy quark with a gauge boson or a charged scalar. In the 5F scheme these processes start with the simplest possible topology, *i.e.*, $2 \rightarrow 1$ at Born level, and feature a b quark as one of the initial-state partons. While not really of prime phenomenological importance as for themselves, 4F and 5F scheme predictions can be easily compared at NLO, and provide a very simple baseline for studying more complex final states.

We then turn to the analysis of t -channel single top production. This probes directly the charged-current interaction of the top quark and it is therefore sensitive to possible new physics associated to the charged-current weak interaction of the top quark. A full calculation of the NLO corrections to W -gluon fusion has been already presented in the literature [86–88], and several schemes have been used. The calculation was originally performed [89, 90] in the 5F scheme. More recently [6, 67] the 4F scheme was adopted in a NLO calculation where a first comparison between 4F and 5F results was performed.

In the last subsection we generalise the results obtained by analysing t -channel single-top and present formulae that can be applied to any b -initiated process, with either one or two b 's in the initial state.

5.1 Associated W and bottom production

Associated production of a W with heavy quarks, such as, charm and bottom, is of great phenomenological importance at the Tevatron as well as the LHC. The production of a W boson and a charm quark, for example, can provide very useful information on the strange content of the proton; it has been subject of measurements at the Tevatron [91] and it is being explored now at the LHC [92]. Wb associated production is also of phenomenological interest, yet its main production mechanism at hadron colliders does not involve a b in the initial state, since at leading order it amounts to W Drell-Yan production with an extra gluon splitting into a $b\bar{b}$ pair.

In this subsection, we consider the simple $2 \rightarrow 1$ processes $u\bar{b} \rightarrow W^+$ and $\bar{u}b \rightarrow W^-$. This is to be considered as a simple alternative, yet fully analogous to, the sample process,

$\bar{b}t \rightarrow H^+$ considered in the seminal work by Olness and Tung [93]. The main difference here is that we focus on the b quark and consider a valence-like PDF in the other initial-state leg, ignoring the suppression originated by the small CKM coupling. In this way, our analysis is not affected by the presence of a sea quark in the initial state.

We first compare the size and the scale dependence of the 4F and 5F predictions at leading and next-to-leading order. Our results are shown in Fig. 6. The 4F curves are obtained using the MCFM code [94], while we have computed the 5F cross sections. We have used the NNPDF2.1 family of parton distribution functions. In particular the default GM-VFN scheme-based set was used for the 5F calculation, and the 4-FFN scheme set was used for the 4F computations. We have considered both the case of the production of a real W boson (first plot in Fig. 6), and that of a virtual one, for two different values of the invariant mass of its decay products, namely 400 GeV (second plot) and 800 GeV (third plot). We take the renormalization and factorization scales to be equal to kM_W , with $0.1 \leq k \leq 3$.

We observe that, for large values of the invariant mass of the W decay products, the 5F cross sections is typically larger than the 4F prediction at the central value $k = 1$. The difference decreases with decreasing k , and the crossing point is around $k \sim 0.1$.

These features can be qualitatively understood by studying the explicit expressions of the leading-order cross sections in the two schemes. At leading-order, the relevant partonic subprocesses for the 5F calculation are

$$b(k_1) + u(k_2) \longrightarrow W(k) \quad (5.1)$$

The corresponding cross-section is

$$\sigma^{5F}(\tau) = \frac{\pi\sqrt{2}}{3} G_F \tau \mathcal{L}_{ub}(\tau, \mu_F^2). \quad (5.2)$$

where $\tau = M_W^2/S$, S is the hadronic centre-of-mass energy squared, and we have set $V_{ub} = 1$. The parton luminosity is given by

$$\mathcal{L}_{ub}(\tau, \mu_F^2) = 2 \int_{\tau}^1 \frac{dz}{z} u^+ \left(\frac{\tau}{z}, \mu_F^2 \right) b(z, \mu_F^2), \quad (5.3)$$

where $u^+ = u + \bar{u}$. As explained in Section 3, the heavy quark parton distribution function $b(z, \mu_F^2)$ arises dynamically as a consequence of Altarelli-Parisi evolution, which resums the leading powers of $\log(\mu_F^2/m_b^2)$ to all orders in perturbation theory. If only the first order of this resummation is retained, one obtains an approximate form for the 5F cross section:

$$\sigma^{5F}(\tau) = \left(\frac{\pi\sqrt{2}}{3} G_F \tau \right) \int_{\tau}^1 \frac{dz}{z} \mathcal{L}_{ug} \left(\frac{\tau}{z}, \mu_F^2 \right) \frac{\alpha_s}{2\pi} P_{qg}(z) \log \frac{\mu_F^2}{m_b^2} + \mathcal{O} \left(\alpha_s^2 \log^2 \frac{\mu_F^2}{m_b^2} \right). \quad (5.4)$$

The choice of factorization scale will be discussed later in this Section. Here we recall from Section 3 that, for fixed μ_F , the size of the neglected terms in Eq. (5.4) is smaller, the smaller is the momentum fraction carried by the b quark. It is therefore interesting to

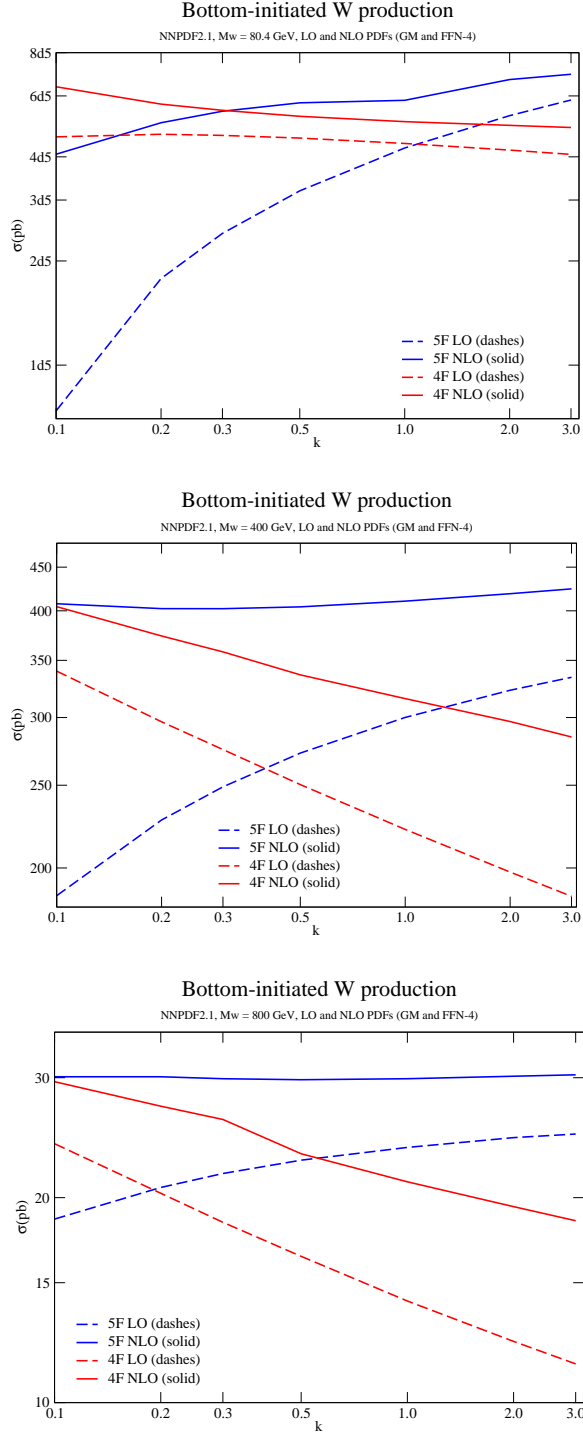


Figure 6. Comparison between 4F and 5F production for b -initiated W production at LHC 14 TeV, as a function of $k = \mu/M_W$, with $\mu = \mu_F = \mu_R$, for $M_W = 80.4$ GeV (top), $M_W = 400$ GeV (middle), $M_W = 800$ GeV (bottom) and $m_b=4.75$ GeV. Input PDFs: NNPDF21_FFNNF4 and NNPDF21 for 4F and 5F respectively.

study the distribution in this variable, for different values of the virtuality of the produced W boson. This distribution is displayed in Fig. 7. We note that the dominant contribution

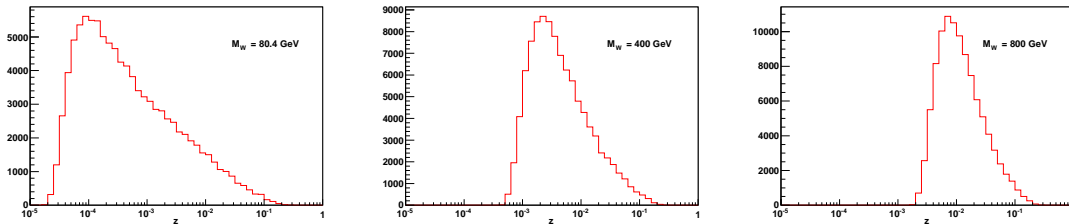


Figure 7. Distribution of the momentum fraction of momentum carried by the b quark(antiquark) in W production initiated by bottom at LHC 14 TeV, LO 5F scheme, for $M_W = 80.4$ GeV (left), $M_W = 400$ GeV (centre), $M_W = 800$ GeV (right). Input PDFs: NNPDF2.1 (LO)

to the convolution integral in Eq. (5.3) comes from very small values of the momentum fraction, ranging from 10^{-4} to 10^{-2} in an order of increasing values of M_W . On the basis of the discussion in Section 3, we conclude that the impact of resummation from Altarelli-Parisi evolution is in this case rather small indeed, apart from very high virtuality of the W .

The factorization scale in the 5F calculation is typically chosen to be the hard scale characteristic of the process, in our case M_W . This is nothing but an order-of-magnitude indication. A less vague indication is given by the comparison with the 4F computation, which we now illustrate. In analogy with the previous case, we consider the subprocesses

$$g(p_1) + u(p_2) \longrightarrow b(p_3) + W(p_4) \quad (5.5)$$

The total cross-section is given by

$$\frac{\sigma^{4F}(\tau)}{\tau} = \int_{\tau}^1 \frac{dz}{z} \mathcal{L}_{ug} \left(\frac{\tau}{z}, \mu_F^2 \right) \frac{\hat{\sigma}^{4F}(z)}{z}, \quad (5.6)$$

where $\tau = \frac{(m_b + M_W)^2}{s}$, $z = \frac{(m_b + M_W)^2}{s}$, $s = (p_1 + p_2)^2$ and

$$\hat{\sigma}^{4F}(z) = \int_{t_-}^{t_+} dt \frac{d\hat{\sigma}}{dt}(s, t, \alpha_s). \quad (5.7)$$

The variable $t = (p_1 - p_3)^2$ represents the collinearity of the bottom pair produced by gluon splitting, and the kinematical bounds are given in Eq. (A.27). The \mathcal{L}_{ug} parton luminosity is defined in Eq. (5.3).

The partonic differential cross section is given in Eq. (A.25). In order to compare the results in the 4F and 5F schemes, it is actually useful to rewrite Eq. (A.25) as a Laurent expansion around $t - m_b^2 = 0$ in order to isolate the collinear singularity, and further neglect

terms which are suppressed by powers of m_b^2/M_W^2 . We find

$$\frac{d\hat{\sigma}}{dt} = \frac{\alpha_s G_F}{6\sqrt{2}s^3} \frac{-2M_W^6 + 2M_W^4 s - M_W^2 s^2}{t - m_b^2} + \mathcal{O}\left(\frac{m_b^2}{M_W^2}\right) + \text{non-singular terms}. \quad (5.8)$$

Since, in this limit,

$$t_- = -(s - M_W^2); \quad t_+ = -\frac{m_b^2 s}{s - M_W^2}, \quad (5.9)$$

the total partonic cross section is

$$\begin{aligned} \hat{\sigma}^{4F}(z) &= \frac{\alpha_s G_F}{6\sqrt{2}s^3} (2M_W^6 - 2M_W^4 s + M_W^2 s^2) \log \left[\frac{s}{m_b^2} \left(1 - \frac{M_W^2}{s}\right)^2 \right] \\ &= \frac{\alpha_s}{2\pi} \left(\pi \frac{\sqrt{2}}{3} G_F \right) z \frac{z^2 + (1-z)^2}{2} \log \left[\frac{M_W^2 (1-z)^2}{m_b^2 z} \right] + \mathcal{O}(m_b^0), \end{aligned} \quad (5.10)$$

where $\mathcal{O}(m_b^0)$ stands for constant or vanishing terms in the limit $m_b \rightarrow 0$. Recalling Eq. (5.6), we can rewrite it as

$$\sigma^{4F}(\tau) = \left(\pi \frac{\sqrt{2}}{3} G_F \tau \right) \int_{\tau}^1 \frac{dz}{z} \mathcal{L}_{ug} \left(\frac{\tau}{z} \right) \frac{\alpha_s}{2\pi} P_{qg}(z) L_{DY} + \mathcal{O}(m_b^0) \quad (5.11)$$

with

$$L_{DY} \equiv \log \left[\frac{M_W^2 (1-z)^2}{m_b^2 z} \right]. \quad (5.12)$$

In order to assess the impact of neglecting non singular terms and the b mass, we have computed the total cross section both with the exact and approximated partonic cross section. The results are $\sigma^{\text{tot}} = 43.7$ nb and $\sigma^{\text{tot}} = 37.6$ nb respectively. In Fig. 8 the density plot of the cross-section is displayed as a function of $1-z$ and $\frac{t_+ - t}{t_+ - t_-}$. It shows that indeed most of the cross section lies in the small- t region, while the points are uniformly distributed in $1-z$. In particular they are not concentrated in the threshold region $z \sim 1$, clearly showing that collinear splitting $g \rightarrow b\bar{b}$ is not a soft effect.

It is now easy to compare Eq. (5.11) with the 5F computation in the approximation of Eq. (5.4). Equations (5.4) and (5.11) have the same structure; they only differ in the argument of the collinear logarithm, which has a fixed value in the case of the 5F calculation, while it depends on the momentum fraction z in the 4F result. In order to estimate the size of the dynamical scale, we have computed the distribution of $(1-z)^2/z$, which is the suppression factor in the argument of the collinear logarithm with respect to M_W/m_b . The result is shown in Fig. 9. We see that this distribution is indeed peaked around values which are sizably smaller than one, and that the peak is shifted to smaller values with increasing M_W .

As a confirmation of the conclusion arising from inspection of Fig. 9, we observe that

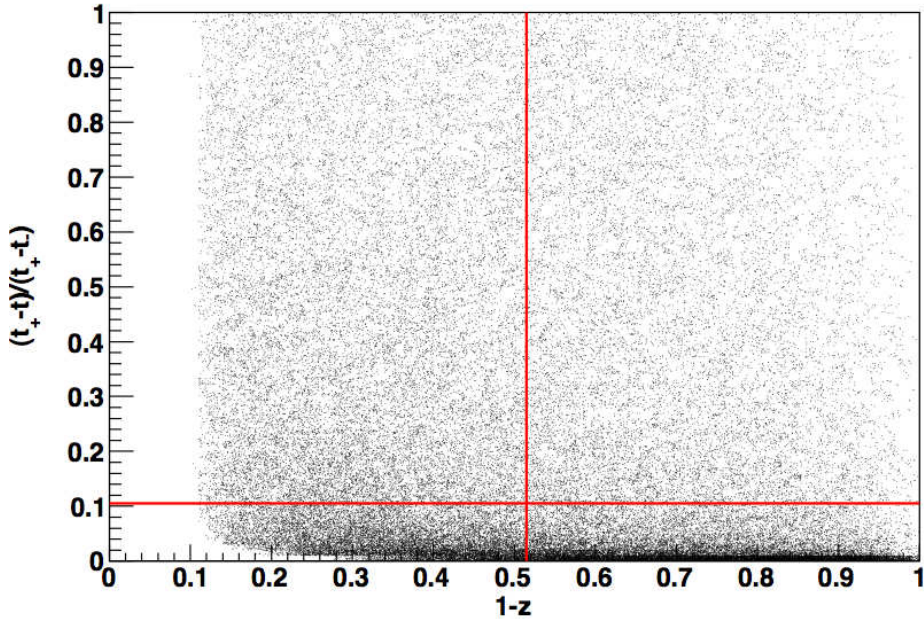


Figure 8. Density plots of the hadronic cross-section of the leading order 4F Wb production at LHC 14 TeV as a function of $1 - z$ and $(t_+ - t)/(t_+ - t_-)$. The straight lines represent the median of the distributions in x and y , respectively.

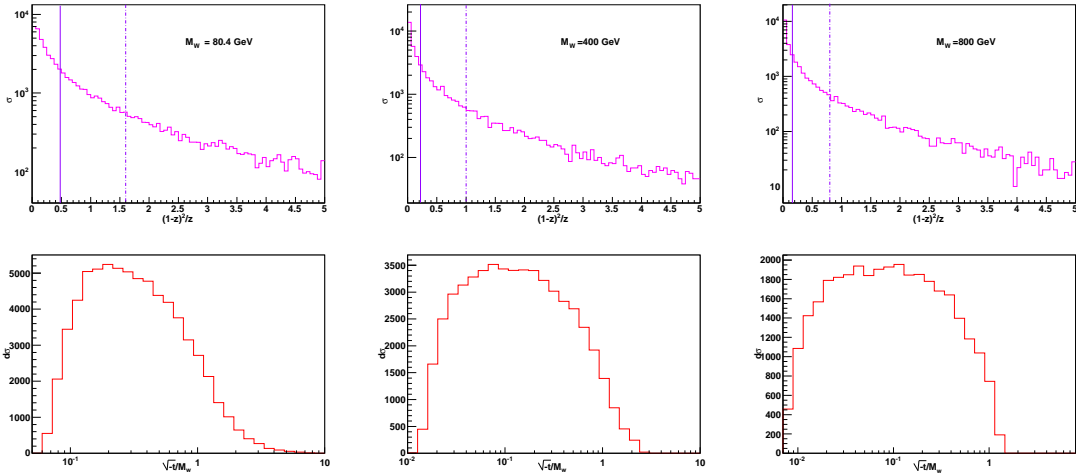


Figure 9. b -initiated W production at the LHC 14 TeV. $M_W = 80.4$ (left), $M_W = 400$ GeV (centre) and $M_W = 800$ GeV (right). **Upper plots:** Distribution of events (in pb/bin) as a function of $Q_{DY}^2(z)/M_W^2 = (1 - z)^2/z$. 50% of the events lie on the left of the vertical solid line, 80% of the events on the left of the vertical dot-dashed line. **Lower plots:** Distribution of events (in pb/bin) as a function of $\log \sqrt{|t|}/M_W$.

the two calculations are seen to give the same result for $\mu_F = \tilde{\mu}_F$, such that

$$\log \frac{\tilde{\mu}_F^2}{m_b^2} = \frac{\int_{\tau}^1 \frac{dz}{z} \mathcal{L}_{ug} \left(\frac{\tau}{z} \right) P_{qg}(z) \log \left[\frac{M_W^2 (1-z)^2}{m_b^2 z} \right]}{\int_{\tau}^1 \frac{dz}{z} \mathcal{L}_{ug} \left(\frac{\tau}{z} \right) P_{qg}(z)}. \quad (5.13)$$

For $\sqrt{S} = 14$ TeV and $M_W = 80.4$ GeV we find

$$\tilde{\mu}_F = 33 \text{ GeV} \quad (\tilde{\mu}_F = 42 \text{ GeV}), \quad (5.14)$$

where the result in parenthesis is obtained by using the exact partonic cross section for the 4F calculation, i.e., keeping the exact m_b and t dependence. Both results point to a value remarkably smaller than M_W , i.e. in the range $\mu_F \simeq [0.4, 0.5] M_W$. This reduction is even more pronounced at larger values of the W virtuality:

$$\begin{aligned} M_W = 400 \text{ GeV} &, & \tilde{\mu}_F &\simeq [0.3, 0.4] M_W \\ M_W = 800 \text{ GeV} &, & \tilde{\mu}_F &\simeq [0.25, 0.35] M_W. \end{aligned} \quad (5.15)$$

The above results clearly suggest that "fair" comparisons between 4F and 5F calculations should be performed at factorization scales that are in general smaller than a naïve choice. This fact had been noticed previously in several studies concerning b -initiated processes, see for instance [30, 37, 68, 95, 96].

Finally, it is instructive to plot the differential cross section as a function of $\log \sqrt{|t|}/M_W$ (lower plots of Fig. 9), i.e., $t d\sigma/dt$. For a massless quark one expects a plateau to develop at small t corresponding to the collinear pole $d\sigma/dt \propto 1/t$. For finite b quark the collinear divergence is regulated by the quark mass and the distribution goes to zero (a.k.a. dead cone). The drop of the plateau at larger t can be taken as signaling the end of the collinear enhanced region, i.e., where the $2 \rightarrow 2$ hard scattering dominates. We observe that in general the collinear plateau drops at scales smaller than M_W for the production of on-shell W bosons, in line with the results found above for the factorization scale. The scale associated to the splitting of the gluon is softer than the scale associated to the hard W production process, which is naturally given by M_W . This implies that the factorization scale that should be set for the bottom PDFs in the four-flavor scheme is smaller than M_W , as suggested in several earlier studies. The considerations in this subsection help to understand the dynamical origin of this fact.

5.2 Single top production

We now consider the production cross-section for events with a single top quark in the final states in hadron-hadron collisions. It was shown in Refs. [6, 67] that the central values of the cross section predicted at next-to-leading order according to the 4F and 5F schemes differ by 5% or less, both at the Tevatron and at the LHC, by setting the factorization scale around the mass of the top quark (or the invariant mass of its decay products). At the Tevatron, the difference is well within the combined uncertainty from higher orders and PDFs, while at the LHC (10 TeV) the consistency was found to be marginal. For larger masses, *i. e.*, for t' production, the differences were found to be much larger. For a t' of mass of 1 TeV, the $2 \rightarrow 2$ prediction is almost twice as large at the Tevatron and 20% larger at the LHC. Therefore, for such large top masses it could well be that the logarithm that is implicitly resummed in the bottom quark distribution function might become relevant, or that an even smaller factorization scale should be used. Here we further investigate this process by using the same procedure adopted in the previous section.

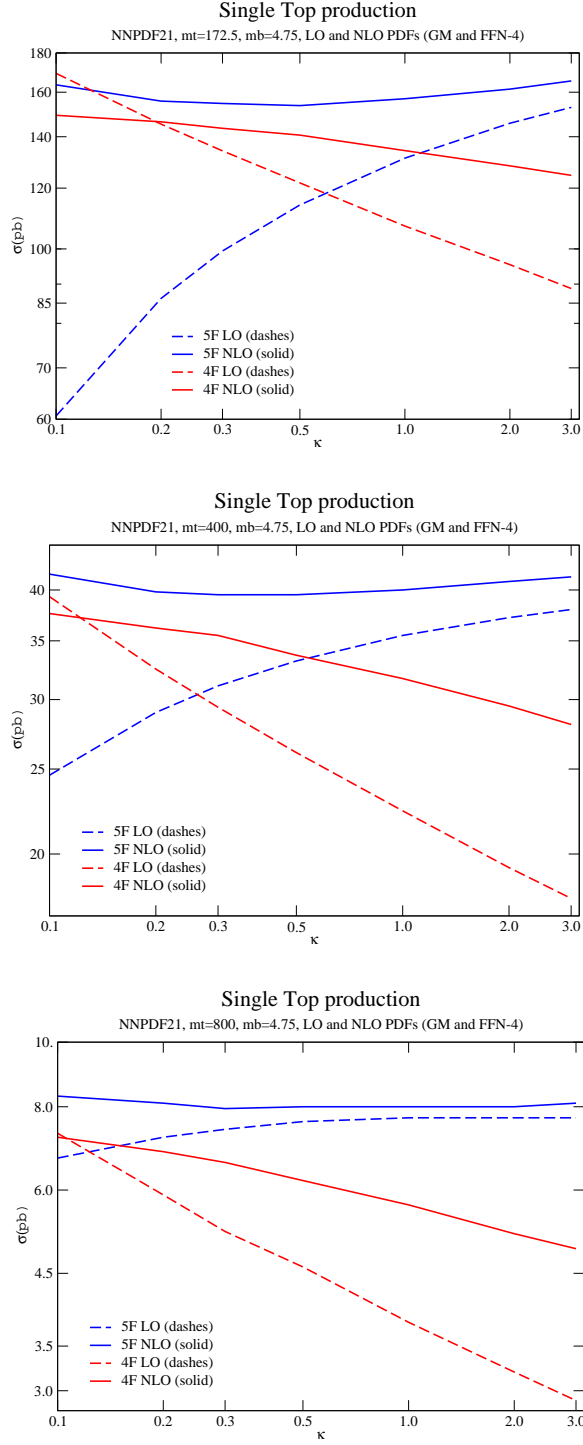


Figure 10. Comparison between 4F and 5F production for single top at LHC 14 TeV as a function of $k = \mu/M_t$, with $\mu = \mu_F = \mu_R$, for $M_t = 172.5$ GeV (top), $M_t = 400$ GeV (middle), $M_t = 800$ GeV (bottom) and $m_b = 4.75$ GeV. Input PDFs: NNPDF21_FF4 and NNPDF21 (LO and NLO) for 4F and 5F respectively.

In Fig. 10 the scale dependence of the total cross section for the single top production in the t -channel is displayed for both the leading and the next-to-leading order computations. For this process the scales are varied about the mass of the top. On top of the on-shell top quark case $M_t = 172.5$ GeV, we consider also two cases where the top has a higher virtuality: $M_t = 400$ GeV and 800 GeV. All curves have been produced by running the MCFM code. In particular, the ACOT computation for the 5F scheme is obtained by matching the LO massive computation with the NLO massless. The input PDFs belong to the NNPDF2.1 family [52]. The set associated to the 5F scheme is the default NNPDF2.1 NLO set, based on a FONLL-A scheme which at NLO is equivalent to the ACOT scheme [51]. The set associated to the 4F scheme is the NNPDF2.1_FF_NF4 set which is based on a 4F fixed flavor number scheme.

In both figures we observe that the LO curves have an opposite behavior, being the 5F curve driven by the scale dependence of the bottom PDFs at the relevant z where the fraction of the momentum is peaked, while the 4F one is driven by the running of α_s . We further observe that both the leading order and the next-to-leading curves obtained in the two schemes are closer to each others for a value of the factorization and renormalization scales which is about half of the mass of the top quark. For heavier top, the scale dependence of the 4F computation deteriorates and the scale at which the two computations get closer decreases as increasing the value of the mass of the top quark.

We first consider the leading-order computation in the 5F scheme. The relevant partonic subprocess is

$$W^*(q) + b(p) \rightarrow t(k), \quad (5.16)$$

and the corresponding amplitude is easily computed:

$$\mathcal{M}_\mu = \frac{g_W}{\sqrt{2}} \bar{u}(k) \gamma^\mu P_L u(p). \quad (5.17)$$

As explained in Appendix A, the contribution to the structure function F_2 is obtained by applying a suitable projection operator on the squared amplitude, and integrating over the one-particle phase space:

$$\begin{aligned} \hat{\sigma}_2^{5F}(z) &= \int d\Phi_1(p+q; k) \left[-\frac{1}{2} g^{\mu\nu} + \frac{3}{2} \frac{4Q^2}{(s+Q^2)^2} p^\mu p^\nu \right] \mathcal{M}_\mu \mathcal{M}_\nu^* \\ &= \pi g_W^2 \delta(1-z), \end{aligned} \quad (5.18)$$

where we have defined, in analogy with deep-inelastic scattering,

$$z = \frac{M_t^2 + Q^2}{s + Q^2}; \quad s = (p+q)^2; \quad Q^2 = -q^2, \quad (5.19)$$

so that $0 \leq z \leq 1$, and we have used

$$d\Phi_1(p+q; k) = \frac{d^3k}{(2\pi)^3 2k^0} (2\pi)^4 \delta(p+q-k) = \frac{2\pi}{s+Q^2} \delta(1-z). \quad (5.20)$$

Thus, at leading order the cross section (or better, the contribution to F_2) from t production is simply proportional to the b parton distribution function. From Fig. 11 we conclude that the fraction of momentum carried by the b quark is peaked at larger value as the virtuality of the produced top increases.

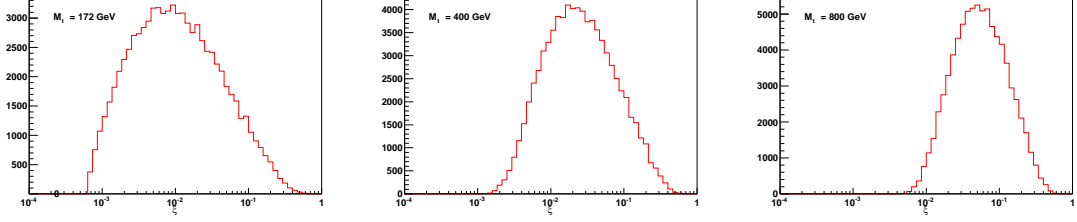


Figure 11. Distributions of events as a function of the proton momentum carried by the incoming b quark in single top production at LHC in the 5F scheme, leading order. $\sqrt{S} = 14$ TeV and $M_t = 172.5$ (left), $M_t = 400$ GeV (centre) and $M_t = 800$ GeV (right). Input PDF: NNPDF21 (LO).

In order to interpret correctly the scale dependence of the curves in Fig. 10 we consider the collinear limit of the massive leading-order computation. The full expression of the LO partonic differential cross-section $d\hat{\sigma}_2^{4F}/dt$ is given by Eqs. (A.8,A.9,A.10) with $M = M_t$, $m = m_b$, $g_R = 0$ and $g_L = g_W/\sqrt{2}$. This specific term in the total cross section is the only one which has a pole in $t = 0$ in the small m_b limit. Taking the limit $m_b \rightarrow 0$ and keeping only terms which give rise to the collinear singularity we find

$$\frac{d\hat{\sigma}_2^{4F}}{dt} = \frac{3\alpha_s g_W^2 C_F}{64(s+Q^2)^3} \left[\frac{(M_t^2 + Q^2)^2 - M_t^2(s+Q^2) - Q^2(s+Q^2) + (s+Q^2)^2/2}{t - m_b^2} \right] + \text{non singular terms.} \quad (5.21)$$

Hence, in this limit,

$$\int_{t_-}^{t_+} dt \frac{d\hat{\sigma}_2^{4F}}{dt} = \frac{3\alpha_s g_W^2 C_F}{128(s+Q^2)^3} [2M_t^4 + 4Q^2 M_t^2 - 2(s+Q^2)M_t^2 + s^2 + Q^4] \log \left[\frac{s}{m_b^2} \left(1 - \frac{M_t^2}{s} \right)^2 \right]. \quad (5.22)$$

With the definition Eq. (5.19), it is immediate to recognize that Eq. (5.22) can be written as

$$\int_{t_{\min}}^{t_{\max}} dt \frac{d\hat{\sigma}_2^{4F}}{dt} = \frac{3\alpha_s g_W^2 C_F}{64(s+Q^2)} \frac{z^2 + (1-z)^2}{2} \log \frac{Q^2(z)}{m_b^2}, \quad (5.23)$$

with

$$Q^2(z) = \frac{(M_t^2 + Q^2)^2}{M_t^2 + (1-z)Q^2} \frac{(1-z)^2}{z}. \quad (5.24)$$

This result can be interpreted as the scale corresponding to the collinear splitting not being M_t or $\sqrt{M_t^2 + Q^2}$, but rather the dynamical scale $Q(z)$. As we will comment at length in

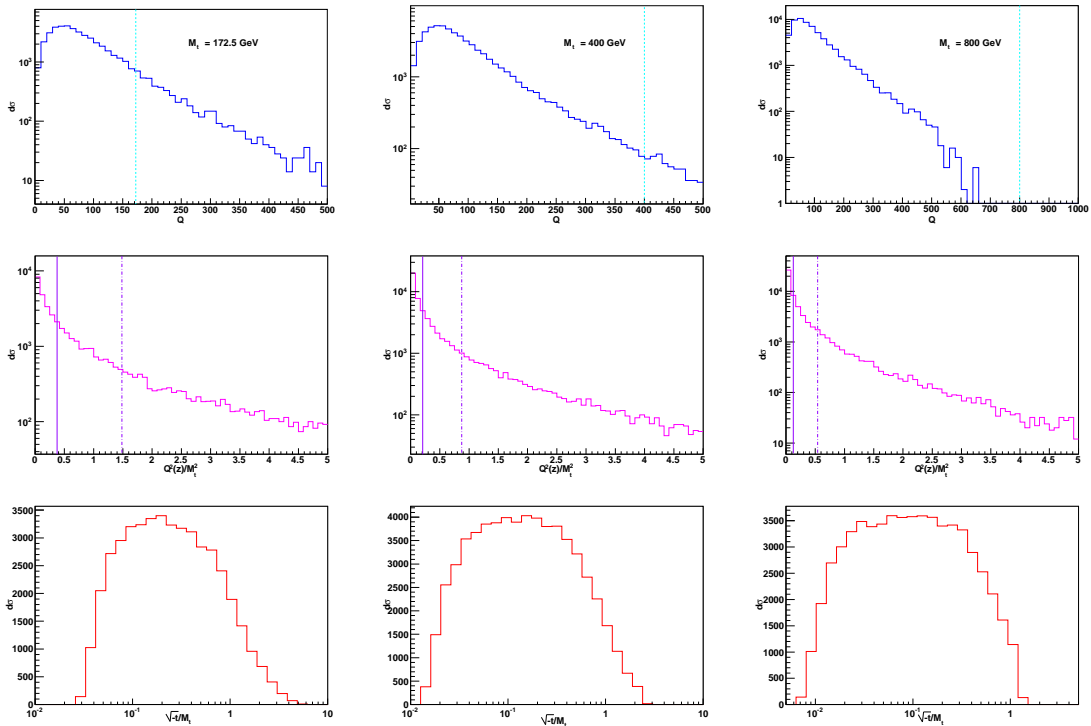


Figure 12. Single-top production at the LHC 14 TeV. Input PDF: NNPDF21_FFN_NF4 (LO). **Top:** Distributions of events as a function of $\sqrt{Q^2}$; the vertical blue line corresponds to $Q = M_t$, for $M_t = 172.5$ (left), $M_t = 400$ GeV (centre) and $M_t = 800$ GeV (right). **Middle:** Distributions of events as a function of $Q^2(z)/M_t^2$, the vertical solid line corresponds to the median of the distribution and the dot-dashed line corresponds to the 80% of the distribution, for $M_t = 172.5$ (left), $M_t = 400$ GeV (centre) and $M_t = 800$ GeV (right). **Bottom:** Distributions of events as a function of $\log \frac{\sqrt{|t|}}{M_t}$ for $M_t = 172.5$ (left), $M_t = 400$ GeV (centre), $M_t = 800$ GeV (right).

the next subsection the expression above actually encompasses all cases discussed so far and paves the way towards the generalisation of our analysis to any process involving one or two b quarks in the initial state. The fact that the collinear logs in single-top production are in fact not very large can be also drawn by looking at the plots in Fig. 12, where cross section distributions are shown as a function of Q , $Q^2(z)/M_t^2$, and $\log \sqrt{|t|}/M_t$, in the first, second and third lines respectively.

5.3 The general case

Single-top production at hadron collisions is not only interesting per se, but also because it provides the simplest yet most general kinematics for any process involving one gluon splitting in the initial state:

$$I(q) + g(p) \rightarrow b(k) + g(k_1) + \dots + g(k_n) + X(P), \quad (5.25)$$

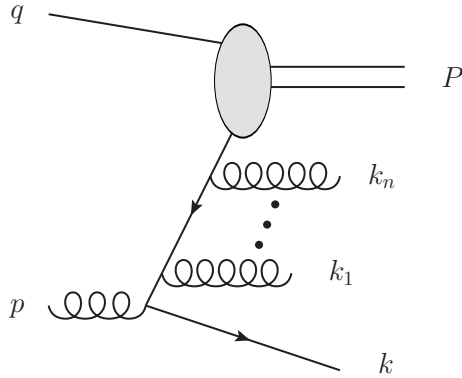


Figure 13. Generic process involving gluon splitting into $b\bar{b}$ pair in the initial state and the production of an heavy system P . Multi-gluon emission from the quark line gives rise to the collinear logarithms at all orders that are resummed into the b parton distribution function.

where I is a generic initial state particle (whose virtuality can also be space-like, such in the case of DIS) and X is a generic heavy system, possibly made out of several particles, such that $P^2 \geq M^2$. The case of single-top production is obtained by identifying I with a virtual W boson with virtuality $q^2 = -Q^2$, and X with a top quark, so that $P^2 \geq M_t^2$. In the case of Wb production, I is a light parton ($q^2 = 0$) and X is a W , so that $P^2 \geq M_W^2$. In both cases, no light parton is present in the final state in the lowest order calculation of the 4F scheme; we have included in Eq. (5.25) the possibility that the system X is produced in association with a collection of light partons with momenta k_1, \dots, k_n , which is obviously the case for higher-order contributions to the cross-section. Multiple gluon emission from the b quark line gives rise to the collinear logs that are resummed in the b -PDF's, Fig. 13.

In the previous sections we have reconsidered the limit $m_b^2 \rightarrow 0$ of the lowest-order 4F cross-sections, which have a collinear singularity due to the gluon splitting into $b\bar{b}$ pair in the initial state; in other words, the b quark mass acts as a regulator of the collinear singularity. Naively, one therefore expects a logarithm of the type

$$L_{\text{naive}} = \log \frac{M^2 + Q^2}{m_b^2} \quad (5.26)$$

i.e., of the hard scale to the collinear regulator, to develop in the integrated cross section. Large M and/or Q therefore motivate the resummation of such logs via the introduction of b -PDF's and the use of the DGLAP equations.

In fact, our analysis based on the lowest-order processes has shown that the logarithmically-enhanced contributions to the cross-sections are proportional to

$$L = \log \frac{Q^2(z)}{m_b^2}, \quad (5.27)$$

where $Q^2(z)$, defined in Eq. (5.24), can be rewritten in the following revelatory form

$$Q^2(z) = (M^2 + Q^2) \frac{(1-z)^2}{z} \frac{1}{1 - \frac{zQ^2}{M^2+Q^2}} \quad \text{with} \quad z = \frac{M^2 + Q^2}{s + Q^2}, \quad (5.28)$$

which encompasses in one expression all interesting cases previously discussed. Equation (5.27) reduces to the log in DIS $b\bar{b}$ production in the limit $M \rightarrow 0$:

$$L_{\text{DIS}} = \log \left[\frac{Q^2}{m_b^2} \frac{1-z}{z} \right] \quad \text{with} \quad z = \frac{Q^2}{s + Q^2}, \quad (5.29)$$

and to the log in the hadronic Wb associated production in the limit $Q^2 \rightarrow 0$:

$$L_{\text{DY}} = \log \left[\frac{M^2}{m_b^2} \frac{(1-z)^2}{z} \right] \quad \text{with} \quad z = \frac{M^2}{s}. \quad (5.30)$$

In the case of single top production, both M^2 and Q^2 are in general non-negligible, and the collinear log keeps its general form Eqs. (5.27-5.28).

In this section we argue that the form Eqs. (5.27-5.28) is not only general enough to encompass all interesting processes at the lowest order, but also it is valid at higher orders, where powers of collinear logarithms are generated by multi-parton emission

$$\log^n \frac{Q_n^2(z)}{m_b^2} \quad (5.31)$$

with $Q_n^2(z) \leq Q^2(z)$ and for processes with two initial-state gluon splitting into $b\bar{b}$.

A complete argument based on the ladder kinematics and valid at any order is detailed in Appendix B. Here we provide an argument that while it has the disadvantage of not providing the exact expression of the cross section in the collinear limit, yet it illustrates in a very simple way the origin and universality of the kinematic terms appearing in Eq. (5.28). For the sake of the argument, we consider the case where X is a real heavy particle, such as a top quark or a W boson.

In the initial-state centre-of-mass system, the four-momenta of the particles in the process Eq. (5.25) can be parametrized as

$$p = \left(\frac{s + Q^2}{2\sqrt{s}}, 0, 0, \frac{s + Q^2}{2\sqrt{s}} \right) \quad (5.32)$$

$$q = \left(\frac{s - Q^2}{2\sqrt{s}}, 0, 0, -\frac{s + Q^2}{2\sqrt{s}} \right) \quad (5.33)$$

$$k_n = (\omega_n, 0, \omega_n \sin \theta, \omega_n \cos \theta) \quad (5.34)$$

$$P_n = \left(\sqrt{\omega_n^2 + M_n^2}, 0, -\omega_n \sin \theta, -\omega_n \cos \theta \right) \quad (5.35)$$

where $P_n = P + k + k_1 + \dots + k_{n-1}$, $P_n^2 = M_n^2$ and

$$\omega_n = \frac{s - M_n^2}{2\sqrt{s}} \leq \frac{\sqrt{s}}{2} \left(1 - \frac{M^2}{s}\right) \quad (5.36)$$

since

$$M_n^2 \geq M^2. \quad (5.37)$$

We may now define

$$z = \frac{M^2 + Q^2}{s + Q^2} \quad (5.38)$$

so that the upper bound on the energy of the gluon with momentum k_n can be written

$$\omega_n \leq \frac{\mathcal{Q}(z)}{2} \quad (5.39)$$

where $\mathcal{Q}(z)$ is given in Eq. (5.28). As a consequence, the transverse momentum of each of the n gluons in the final state is bound from above by the same quantity. We therefore expect at most a factor of

$$\log \frac{\mathcal{Q}^2(z)}{m_b^2} \quad (5.40)$$

for each emitted gluon. This covers all processes that involve one gluon splitting in the initial state. In fact, given that no use on the details of the kinematics is made, the same argument can be equally applied to processes such as $gg \rightarrow Zb\bar{b}$ or $gg \rightarrow Hb\bar{b}$ that involve two gluons splitting into $b\bar{b}$ pairs in the initial state. A detailed proof in terms of t -channel kinematics is provided for this case too in Appendix B.

We conclude this section by noting that while the impact of the logarithms for processes with one or two $g \rightarrow b\bar{b}$ splittings in the initial state is similar, the correspondence between LO, NLO,... 4F calculations with the LL, NLL,...accuracy of calculations in 5F schemes only applies to processes with only one splitting. This simple relation does not hold in the case of two splittings as for example in $gg \rightarrow Hb\bar{b}$. At LO, the 4F calculation displays the leading logs $\alpha_s^2 \log^2 \frac{Q^2(z)}{m_b^2}$ and part of the subleading ones, yet at NLO only one splitting at a time is correctly reproduced up to NLL the other being effectively only LL. In other words, one would need to go up to NNLO in the 4F scheme to correctly account for all NLL terms of each splitting at that order. This is easily achieved by the 5F calculation already at NLO. In this respect it is not surprising that 5F scheme calculations of total cross sections for $b\bar{b}$ fusion into Higgs or Z leads to very stable results under scale variations [73].

6 Conclusions

A quite important set of processes that feature gluon splitting into a $b\bar{b}$ pair in the initial state are of phenomenological interest at the LHC. Accurate predictions for such processes can be obtained performing calculations in either the 4F and 5F schemes. Motivated by the somewhat unexpected result that in most cases predictions in the two schemes are found

to substantially agree within uncertainties if judicious scale choices are made, in this work we have addressed the following two basic questions:

- What is the typical size of the effects of the resummation of initial-state collinear logs of the type $\log \frac{Q^2}{m_b^2}$ with respect to an approximation where only logs at a finite order in perturbation theory are kept?
- What is the typical size of the $\log \frac{Q^2}{m_b^2}$ themselves in phenomenologically relevant processes at hadron colliders, and in particular at the LHC?

Our main conclusion is that unless the typical Bjorken x probed by the process is large, the effects of initial-state collinear $\log \frac{Q^2}{m_b^2}$'s is always modest, and that even though total cross-sections computed in 5-flavor schemes may indeed display a smaller uncertainty, such logarithms do not spoil the convergence of perturbation theory in 4-flavor scheme calculations.

We have identified two main and different reasons, one of dynamical and the other of kinematical nature.

The first is that the effects of the resummation of the $\log \frac{Q^2}{m_b^2}$ universal terms is quite small and relevant mainly at large Bjorken x and in general keeping only the explicit logs appearing at NLO is in fact an excellent approximation. This observation accounts for previously noticed, and yet not well-understood, behaviours, such as the more sizable differences between predictions in the two schemes for single top and $bb \rightarrow H$ at the Tevatron than at the LHC [67, 68].

The second result of our study is that the effective scale Q which enters in the initial-state collinear logarithm while proportional to hardest scale(s) in the process, turns out to be modified by universal phase space factors that tend to reduce the size of the logarithms for processes taking place at hadron colliders. In our study we have provided a simple analytic formula, valid also in the case of processes with two b quarks in the initial state, that can be used to quantitatively assess the size of such logs for any process at the LHC. We have also provided a simple rule to choose the factorization scale where to perform comparisons between calculations in the two schemes. As a result, a consistent and quantitative explanation is provided of the many examples where a substantial agreement between total cross sections obtained at NLO (and beyond) in the two schemes can be found within the expected uncertainties.

The main outcome of this study is that 4F and 5F schemes provide complementary information and it strongly motivates having calculations at higher orders available in both schemes for any given process. (Improved) 5-flavor schemes, for example, can typically provide quite accurate predictions for total rates and being simpler, in some cases allow the calculations to be performed at NNLO, such as those already available for $bb \rightarrow H, Z$ and foreseeable in the near future, such as t -channel single-top production. On the other hand, being often the effects of resummation very mild, 4-flavor calculations can be also put to use. They can be useful to achieve accurate fully exclusive predictions, such as those obtained from Monte Carlo programs at NLO accuracy. Promoting a 4-flavor calculation at NLO to an event generator is nowadays a fully automatic procedure and kinematic effects

due to the b quark mass can be taken into account from the start leading for example to a more accurate description of the kinematics of the spectator b quarks in all phase space.

As we have argued, processes that can be described by two b quarks in the initial state, such as $pp \rightarrow Hbb$ and $pp \rightarrow Zbb$ entail a simple extension of our approach. The comparison between the 5F and 4F schemes can be performed at NNLO for the former and NLO level for the latter and results could be compared with alternative approaches, such as the proposal of Ref. [97]. We leave this to future work. In addition, given the absence of any phenomenological motivation for an intrinsic charm contribution to the proton, it would be certainly interesting to investigate to which extent the results obtained here for b quarks can be applied to c quarks. On a more speculative level, one could also wonder whether the approach followed in this work could be employed to develop a criterium for an optimal central factorization scale choice for processes at the LHC. We have argued that initial state collinear logs display a universal form valid at all orders which in fact is independent of the details of splitting as well as of the hard scattering, but only due to phase space. This suggests that for arbitrary processes with light partons in the initial state collinear logs are of the form $\log \frac{\mathcal{Q}^2(z)}{\Lambda_{\text{QCD}}^2}$ and therefore factorization scales chosen on event-by-event basis as $\mu_F \simeq \mathcal{Q}(z)$ would lead to an improvement of the perturbative expansion. Developments in this direction would be certainly welcome.

Acknowledgements

We would like to thank Scott Willenbrock and Stefano Forte for many useful discussions on this topic and for comments on this work. F.M. is thankful for the always lively discussions on heavy-quark PDF's to Francesco Tramontano, Fred Olness, John Campbell, Michael Kraemer, Michael Spira, Michelangelo Mangano, Paolo Nason, and Robert Harlander. F.M. and M.U.'s work is partially supported by the Belgian IAP Program, BELSPO P6/11-P and IISN conventions. M.U. is supported by the Bundesministerium für Bildung and Forschung (BmBF) of the Federal Republic of Germany (project code 05H09PAE).

A LO matrix elements for heavy quark production

In this Appendix we give the explicit expressions for leading order partonic cross sections relevant for Wb production and tb production.

A.1 Heavy quark production (DIS and single top)

We first consider the production of a heavy quark Q_m of mass m in association with another heavy quark Q_M of mass M (with $M \geq m$). In the 4F scheme the heavy quark of mass m is treated as a massive final state and does not contribute to the proton wave function. The relevant leading-order partonic subprocess is

$$g(p) + B^*(q) \rightarrow \bar{Q}_m(k_1) + Q_M(k_2). \quad (\text{A.1})$$

The results presented in this Appendix are relevant both for the calculation of electro-production cross sections, where the virtual vector boson B^* is assumed to be radiated by

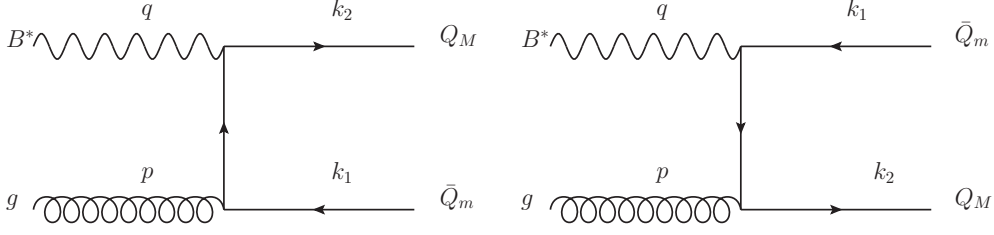


Figure 14. LO Feynman diagrams associated to the $Q_M \bar{Q}_m$ production

an incoming lepton, and for hadroproduction, where the vector boson is exchanged with a light quark. The process is depicted in Fig. 2. The amplitude in the 4F scheme is obtained from the diagrams displayed in figure 14. We define

$$\begin{aligned}
t &= (p - k_1)^2 = m^2 - 2p \cdot k_1, \\
u &= (p - k_2)^2 = M^2 - 2p \cdot k_2, \\
s &= (p + q)^2 = 2p \cdot q - Q^2.
\end{aligned} \tag{A.2}$$

For a generic coupling between the vector boson B and the heavy quarks,

$$g\Gamma^\mu \equiv g_R \gamma^\mu \frac{1 + \gamma_5}{2} + g_L \gamma^\mu \frac{1 - \gamma_5}{2} \tag{A.3}$$

the matrix element \mathcal{M}^μ reads

$$\mathcal{M}^\mu = -i g g_s t_c \bar{u}(k_2) \left[\Gamma^\mu \frac{\not{p}' - \not{k}_1 + m}{t - m^2} \gamma^\alpha + \gamma^\alpha \frac{\not{k}_2 - \not{p}' + M}{u - M^2} \Gamma^\mu \right] v(k_1) \epsilon_\alpha(p). \tag{A.4}$$

The transverse, longitudinal and axial components of the squared amplitude can be isolated by suitable projection operators. We define

$$\mathcal{M}_G = -\frac{1}{2} g^{\mu\nu} \mathcal{M}_\mu \mathcal{M}_\nu^* \tag{A.5}$$

$$\mathcal{M}_L = \frac{4Q^2}{(s + Q^2)^2} p^\mu p^\nu \mathcal{M}_\mu \mathcal{M}_\nu^* \tag{A.6}$$

$$\mathcal{M}_3 = -i \frac{2Q^2}{(s + Q^2)^2} \varepsilon_{\mu\nu\sigma\rho} p^\sigma q^\rho \mathcal{M}_\mu \mathcal{M}_\nu^*. \tag{A.7}$$

We find

$$\mathcal{M}_G = \frac{2g_s^2 C_F}{t_1^2 u_1^2} \left\{ (g_L^2 + g_R^2) \left[+ 2m^2 M^2 s_1^2 - 2s_1 [m^4 u_1 + M^4 t_1 + (m^2 + M^2) u_1 t_1] \right. \right. \\ \left. \left. + t_1 u_1 (2Q^4 - 2s_1 Q^2 + t_1^2 + u_1^2) + 2Q^2 [m^2 u_1 (2t_1 + u_1) + M^2 t_1 (2u_1 + t_1)] \right] \right. \\ \left. + 16g_L g_R m M \left[s_1 (u_1 m^2 + t_1 M^2) + u_1 t_1 (s_1 - Q^2) \right] \right\} \quad (\text{A.8})$$

$$\mathcal{M}_L = \frac{16g_s^2 C_F Q^2 (g_L^2 + g_R^2)}{s_1^2 t_1 u_1} \left[s_1 (u_1 m^2 + t_1 M^2) + u_1 t_1 (s_1 - Q^2) \right] \quad (\text{A.9})$$

$$\mathcal{M}_3 = \frac{4g_s^2 C_F Q^2 (g_L^2 - g_R^2)}{s_1^2 t_1^2 u_1^2} \left[2s_1^2 (M^4 t_1 - m^4 u_1) + 2s_1 m^2 M^2 (t_1^2 - u_1^2) \right. \\ \left. + 2s_1 Q^2 (M^2 t_1^2 - m^2 u_1^2) - 2s_1 u_1 t_1 (-s_1 + 2Q^2) (M^2 - m^2) \right. \\ \left. - t_1 u_1 (t_1 - u_1) (2Q^4 - 2Q^2 s_1 + s_1^2) \right] \quad (\text{A.10})$$

where $t_1 = t - m^2$, $u_1 = u - M^2$ and $s_1 = s + Q^2$. The two-body invariant phase space measure is given by

$$d\Phi_2 = \frac{d^3 k_1}{(2\pi)^3 2E_1} \frac{d^3 k_2}{(2\pi)^3 2E_2} (2\pi)^4 \delta^{(4)}(p + q - k_1 - k_2) = \frac{1}{8\pi s_1} dt \quad (\text{A.11})$$

and therefore, by definition, [98]

$$\frac{d\hat{\sigma}_G^{4\text{F}}}{dt} = \frac{1}{64s_1} \frac{1}{8\pi s_1} \mathcal{M}_T \quad (\text{A.12})$$

$$\frac{d\hat{\sigma}_L^{4\text{F}}}{dt} = \frac{1}{32s_1} \frac{1}{8\pi s_1} \mathcal{M}_L \quad (\text{A.13})$$

$$\frac{d\hat{\sigma}_3^{4\text{F}}}{dt} = \frac{1}{64s_1} \frac{1}{8\pi s_1} \mathcal{M}_3. \quad (\text{A.14})$$

The partonic cross-section

$$\frac{d\hat{\sigma}_2^{4\text{F}}}{dt} = \frac{d\hat{\sigma}_G^{4\text{F}}}{dt} + \frac{3}{2} \frac{d\hat{\sigma}_L^{4\text{F}}}{dt} \quad (\text{A.15})$$

has singularities for $t \rightarrow 0$ in the limit $m \rightarrow 0$ and for $u \rightarrow 0$ in the limit $M \rightarrow 0$. The amplitudes Eqs. (A.8,A.9,A.10) are manifestly symmetric under the exchange $t_1 \leftrightarrow u_1$, $M \leftrightarrow m$.

In case of DIS ($g_R = g_L = e_b \sqrt{4\pi\alpha_e}$, $M = m = m_b$) Eq. (A.15) reads

$$\frac{d\hat{\sigma}_2^{4F}}{dt} = \frac{\alpha_s C_F \pi \alpha_e e_H^2}{8s_1^4 t_1^2 u_1^2} \left[4m_b^2 s_1^4 + 2m_b^2 s_1^2 (14t_1 u_1 Q^2 - s) 1^2 Q^2 - 2s_1 t_1 u_1 \right. \\ \left. - t_1 u_1 [24Q^2 t_1 u_1 (s_1 - Q^2) + s_1^2 (2Q^4 - 2Q^2 s_1 + s_1^2 - 2t_1 u_1)] \right], \quad (\text{A.16})$$

where $e_b = -1/3$ is the electric charge of the bottom quark.

In case of single top ($g_R = 0$, $g_L = g_w/\sqrt{2}$, $M = M_t$ and $m = m_b$) Eq. (A.15) reads

$$\frac{d\hat{\sigma}_2^{4F}}{dt} = \frac{\alpha_s C_F g_w^2}{128s_1^4 t_1^2 u_1^2} \left[2s_1^3 (m_b^4 u_1 + M_t^4 t_1) - 2s_1^4 m_b^2 M_t^2 \right. \\ + 4(M_t^2 t_1 + m_b^2 u_1) (s_1^3 Q^2 - 6Q^2 t_1 u_1 s_1) + 2s_1^2 t_1 u_1 (s_1 - 2Q^2) (m_b^2 + M_t^2) \\ \left. + s_1^2 u_1 t_1 (2Q^4 - 2Q^2 s_1 + s_1^2 - 2t_1 u_1) - 24Q^2 t_1^2 u_1^2 (s_1 - Q^2) \right]. \quad (\text{A.17})$$

Choosing the partonic centre-of-mass frame of the B^*g system, the explicit expressions of the four-momenta are

$$p = \left(\frac{s + Q^2}{2\sqrt{s}}, 0, 0, -\frac{s + Q^2}{2\sqrt{s}} \right) \\ q = \left(\frac{s - Q^2}{2\sqrt{s}}, 0, 0, \frac{s + Q^2}{2\sqrt{s}} \right) \\ k_1 = \left(E_1, 0, |\vec{k}| \sin \theta, |\vec{k}| \cos \theta \right) \\ k_2 = \left(E_2, 0, -|\vec{k}| \sin \theta, -|\vec{k}| \cos \theta \right),$$

where E_1, E_2 and $|\vec{k}|$ are fixed by energy-momentum conservation and mass-shell relations:

$$|\vec{k}|^2 = \frac{\lambda(s, M^2, m^2)}{4s} \\ E_1 = \frac{s + m^2 - M^2}{2\sqrt{s}} \\ E_2 = \frac{s - m^2 + M^2}{2\sqrt{s}} \quad (\text{A.18})$$

where $\lambda(a, b, c) = a^2 + b^2 + c^2 - 2ab - 2ac - 2bc$.

The masses of the heavy quarks act as regulators of collinear singularities, originated by poles in t_1, u_1 in the squared amplitudes. Since $t_- \leq t \leq t_+$, with

$$t_{\pm} = m^2 - \frac{s + Q^2}{2s} \left(s + m^2 - M^2 \mp \lambda^{\frac{1}{2}}(s, M^2, m^2) \right) \quad (\text{A.19})$$

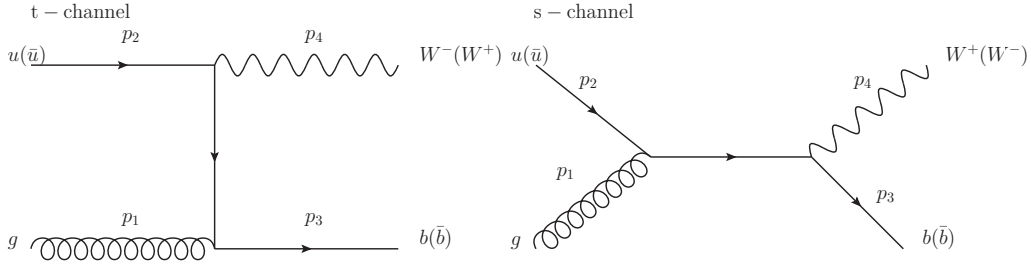


Figure 15. LO Feynman diagrams associated to the t - and s - channel Wb production

we find

$$L_t = \int_{t_-}^{t_+} \frac{dt}{t - m^2} = \log \frac{s + m^2 - M^2 + \lambda^{\frac{1}{2}}(s, M^2, m^2)}{s + m^2 - M^2 - \lambda^{\frac{1}{2}}(s, M^2, m^2)}, \quad (\text{A.20})$$

and

$$L_u = \int_{t_-}^{t_+} \frac{dt}{u - M^2} = \log \frac{s + M^2 - m^2 + \lambda^{\frac{1}{2}}(s, M^2, m^2)}{s + M^2 - m^2 - \lambda^{\frac{1}{2}}(s, M^2, m^2)}. \quad (\text{A.21})$$

In the limit $m^2 \ll M^2$, relevant for single top production, we have

$$L_t \rightarrow \log \left[\frac{s}{m^2} \left(1 - \frac{M^2}{s} \right)^2 \right] \quad L_u \rightarrow \log \frac{s}{M^2}, \quad (\text{A.22})$$

whereas for $m^2 = M^2 \rightarrow 0$ as in the case of $b\bar{b}$ or $c\bar{c}$ production, we find

$$L_t = L_u \rightarrow \log \frac{s}{m^2}. \quad (\text{A.23})$$

A.2 Associated Wb production

We now consider associated Wb production. In the simplified case in which only one light quark appears in the initial state, e.g. the u quark, the relevant leading-order subprocesses are

$$\begin{aligned} g(p_1) + \bar{u}(p_2) &\longrightarrow \bar{b}(p_3) + W^-(p_4) \\ g(p_1) + u(p_2) &\longrightarrow b(p_3) + W^+(p_4) \end{aligned} \quad (\text{A.24})$$

and the LO Feynman diagrams are shown in figure 15. We define

$$\begin{aligned} s &= (p_1 + p_2)^2 = 2p_1 \cdot p_2 \\ t &= (p_1 - p_3)^2 = m_b^2 - 2p_1 \cdot p_3 \\ u &= (p_2 - p_3)^2 = m_b^2 - 2p_2 \cdot p_3. \end{aligned}$$

This process is related to the one discussed above by crossing, namely

$$t \leftrightarrow s \quad u \leftrightarrow t \quad s \leftrightarrow u.$$

Therefore the transversal, longitudinal and axial components of the squared matrix elements can be obtained from Eqs. (A.8,A.9,A.10) by setting $g_R = 0$, $g_L = g_w/\sqrt{2}$, $m = 0$, $M = m_b$ and by crossing the kinematic variables according to the above equation. The partonic differential cross section is given by

$$\begin{aligned} \frac{d\hat{\sigma}^{4F}}{dt} = & \frac{\alpha_s G_F}{12\sqrt{2}s^3 (t - m_b^2)^2} \left[m_b^8 - m_b^6(2s + t) - m_b^4 (2M_W^4 + 2M_W^2 t - (s + t)^2) \right. \\ & - m_b^2 \left(-4M_W^6 + 2M_W^4 t - 2M_W^2 (s^2 - st + 2t^2) + t(s + t)^2 \right) \\ & \left. - 2M_W^2 t (2M_W^4 - 2M_W^2(s + t) + s^2 + t^2) \right]. \end{aligned} \quad (\text{A.25})$$

In the partonic centre of mass frame we can write the 4-momenta of the particles as

$$\begin{aligned} p_1 &= \left(\frac{\sqrt{s}}{2}, 0, 0, \frac{\sqrt{s}}{2} \right) \\ p_2 &= \left(\frac{\sqrt{s}}{2}, 0, 0, -\frac{\sqrt{s}}{2} \right) \\ p_3 &= (E_3, 0, |\vec{p}| \sin \theta, |\vec{p}| \cos \theta) \\ p_4 &= (E_4, 0, -|\vec{p}| \sin \theta, -|\vec{p}| \cos \theta) \end{aligned}$$

where, by the energy–momentum conservation,

$$\begin{aligned} |\vec{p}| &= \frac{\lambda^{\frac{1}{2}}(s, M_W^2, m_b^2)}{2\sqrt{s}} \\ E_3 &= \frac{s + m_b^2 - M_W^2}{2\sqrt{s}} \\ E_4 &= \frac{s + M_W^2 - m_b^2}{2\sqrt{s}}. \end{aligned} \quad (\text{A.26})$$

The 4F LO partonic cross section is readily obtained by integration in the range $t_- \leq t \leq t_+$, with

$$\begin{aligned} t_- &= m_b^2 - \frac{1}{2} \left[s + m_b^2 - M_W^2 + \lambda^{\frac{1}{2}}(s, m_b^2, M_W^2) \right] \\ t_+ &= m_b^2 - \frac{1}{2} \left[s + m_b^2 - M_W^2 - \lambda^{\frac{1}{2}}(s, m_b^2, M_W^2) \right]. \end{aligned} \quad (\text{A.27})$$

The dominant contribution in the collinear limit $t \rightarrow 0, m_b \rightarrow 0$ is therefore proportional to

$$L = \log \frac{t_+ - m_b^2}{t_- - m_b^2} \rightarrow \log \frac{(s - M_W)^2}{m_b^2 s}. \quad (\text{A.28})$$

B Higher orders

In Section 5.3 we have considered the general class of processes

$$I(q) + g(p) \rightarrow b(k) + g(k_1) + \dots + g(k_n) + X(P), \quad (\text{B.1})$$

where X is a generic heavy system, such that $P^2 \geq M^2$. By using a simple argument we have shown that transverse momentum of each of the n gluons in the final state is bounded from above by the same quantity and therefore expect a factor of

$$\log \frac{Q^2(z)}{m_b^2} \quad (\text{B.2})$$

for each emitted gluon.

This simple argument has the disadvantage that it does not provide us with the exact expression of the cross section in the collinear limit. The argument can be made more precise by studying the explicit expression of the squared amplitude and of the phase space measure for multiparton emission in the collinear limit. In order to simplify our discussion, we specialize to the case when X is a real heavy particle, such as a top quark or a W boson.

The dominant Feynman diagrams in the collinear limit are shown in Fig. 13.

It will therefore be convenient to express both the squared amplitude and the phase space measure in terms of the variables

$$\begin{aligned} t &= (p - k)^2 \\ t_1 &= (p - k - k_1)^2 \\ &\dots \\ t_n &= (p - k - k_1 - \dots - k_n)^2 \end{aligned} \quad (\text{B.3})$$

because the leading contribution to the squared amplitude in the collinear limit will be proportional to

$$\frac{1}{t - m_b^2} \frac{1}{t_1 - m_b^2} \dots \frac{1}{t_n - m_b^2}. \quad (\text{B.4})$$

The $(n + 2)$ -body phase space measure can be worked out by the usual factorization technique [99]. We obtain

$$d\Phi_{n+2}(p, q; k, k_1, \dots, k_n, P) = \int_{M^2}^{(\sqrt{s} - m_b)^2} \frac{dM_n^2}{2\pi} d\Phi_2(p, q; k, P_n) d\Phi_{n+1}(P_n; k_1, \dots, k_n, P), \quad (\text{B.5})$$

where

$$P_n = k_1 + \dots + k_n + P; \quad P_n^2 = M_n^2. \quad (\text{B.6})$$

In the reference frame defined by Eqs. (5.32) and (5.33) we have

$$d\Phi_2(p, q; k, P_n) = \frac{1}{16\pi^2} \frac{|\vec{k}|}{\sqrt{s}} d\phi d\cos\theta, \quad (\text{B.7})$$

where θ, ϕ are the polar and azimuthal angles of \vec{k} , and

$$|\vec{k}|^2 = \frac{\lambda(s, m_b^2, M_n^2)}{4s}. \quad (\text{B.8})$$

Because

$$t = (p - k)^2 = m_b^2 - \frac{s + Q^2}{\sqrt{s}} \left(\sqrt{m_b^2 + |\vec{k}|^2} - |\vec{k}| \cos \theta \right), \quad (\text{B.9})$$

we may recast Eq. (B.7) in the Lorentz-invariant form

$$d\Phi_2(p, q; k, P_n) = \frac{1}{16\pi^2} \frac{dt}{s + Q^2} d\phi. \quad (\text{B.10})$$

The kinematic bounds on t are easily read off Eqs. (B.8, B.9):

$$t^- \leq t \leq t^+ \\ t^\mp = m_b^2 - \frac{s + Q^2}{2s} \left[s + m_b^2 - M_n^2 \pm \lambda^{\frac{1}{2}}(s, m_b^2, M_n^2) \right]. \quad (\text{B.11})$$

The factorization procedure can be iterated until the whole phase space is expressed as a product of two-body phase space measures. Let us take one more step explicitly:

$$d\Phi_{n+1}(P_n; k_1, \dots, k_n, P) = \int_{M^2}^{M_n^2} \frac{dM_{n-1}^2}{2\pi} d\Phi_2(P_n; k_1, P_{n-1}) d\Phi_n(P_{n-1}; k_2, \dots, k_n, P), \quad (\text{B.12})$$

where

$$P_{n-1} = k_2 + \dots + k_n + P; \quad P_{n-1}^2 = M_{n-1}^2. \quad (\text{B.13})$$

Choosing

$$p - k = \left(\sqrt{t + \omega^2}, 0, 0, \omega \right) \quad (\text{B.14})$$

$$q = \left(\sqrt{q^2 + \omega^2}, 0, 0, -\omega \right) \quad (\text{B.15})$$

the condition $(p - k + q)^2 = M_n^2$ gives

$$\omega = \frac{\lambda^{\frac{1}{2}}(M_n^2, t, q^2)}{2M_n}. \quad (\text{B.16})$$

A straightforward calculation yields

$$t_1 = (p - k - k_1)^2 = t - \frac{M_n^2 - M_{n-1}^2}{2M_n^2} \left[M_n^2 + t - q^2 - \lambda^{\frac{1}{2}}(M_n^2, t, q^2) \cos \theta_1 \right] \quad (\text{B.17})$$

so that

$$d\Phi_2(P_n; k_1, P_{n-1}) = \frac{1}{16\pi^2} \frac{dt_1}{\lambda^{\frac{1}{2}}(M_n^2, t, q^2)} d\phi_1 \quad (\text{B.18})$$

with

$$t_1^- \leq t_1 \leq t_1^+ \\ t_1^\mp = t - \frac{M_n^2 - M_{n-1}^2}{2M_n^2} \left[M_n^2 + t - q^2 \pm \lambda^{\frac{1}{2}}(M_n^2, t, q^2) \right]. \quad (\text{B.19})$$

Thus

$$d\Phi_{n+2}(p, q; k, k_1, \dots, k_n, P) = \int_{M^2}^{(\sqrt{s}-m_b)^2} \frac{dM_n^2}{2\pi} \frac{1}{(4\pi)^2} \frac{dt}{s+Q^2} d\phi \\ \int_{M^2}^{M_n^2} \frac{dM_{n-1}^2}{2\pi} \frac{1}{(4\pi)^2} \frac{dt_1}{\lambda^{\frac{1}{2}}(M_n^2, t, q^2)} d\phi_1 d\Phi_n(P_{n-1}; k_2, \dots, k_n, P). \quad (\text{B.20})$$

The procedure can be iterated, to obtain

$$d\Phi_{n+2}(p, q; k, k_1, \dots, k_n, P) = \frac{1}{(2\pi)^n} \frac{1}{(4\pi)^{2n+2}} d\phi d\phi_1 \dots d\phi_n \\ \int_{M^2}^{(\sqrt{s}-m_b)^2} dM_n^2 \int_{M^2}^{M_n^2} dM_{n-1}^2 \dots \int_{M^2}^{M_2^2} dM_1^2 \\ \frac{dt}{s+Q^2} \int_{t^-}^{t^+} \frac{dt_n}{\lambda^{\frac{1}{2}}(M_1^2, t_{n-1}, q^2)} \int_{t_n^-}^{t_n^+} \frac{dt_{n-1}}{\lambda^{\frac{1}{2}}(M_2^2, t_{n-2}, q^2)} \dots \int_{t_1^-}^{t_1^+} \frac{dt_1}{\lambda^{\frac{1}{2}}(M_n^2, t, q^2)} \quad (\text{B.21})$$

with

$$t_j^- \leq t_j \leq t_j^+ \\ t_j^\mp = t_{j-1} - \frac{M_{n-j+1}^2 - M_{n-j}^2}{2M_{n-j+1}^2} \left[M_{n-j+1}^2 + t_{j-1} - q^2 \pm \lambda^{\frac{1}{2}}(M_{n-j+1}^2, t_{j-1}, q^2) \right] \quad (\text{B.22})$$

for $1 \leq j \leq n$, where we understand that $t_0 \equiv t$, $M_0 \equiv M$.

Our next task is evaluating the most singular term in the cross section, σ^{coll} , in the limit $m_b \rightarrow 0$. This is obtained by integrating the squared amplitude, Eq. (B.4), using the integration measure Eq. (B.21). Let us consider the case $n = 1$ as an example. In this case

$$\sigma^{\text{coll}} = \int_{M^2}^{(\sqrt{s}-m_b)^2} dM_1^2 \int_{t^-}^{t^+} dt \frac{1}{t - m_b^2} \frac{1}{\lambda^{\frac{1}{2}}(M_1^2, t, q^2)} \int_{t_1^-}^{t_1^+} \frac{dt_1}{t_1 - m_b^2} \\ = \int_{M^2}^{(\sqrt{s}-m_b)^2} dM_1^2 \int_{t^-}^{t^+} dt \frac{1}{t - m_b^2} \frac{1}{\lambda^{\frac{1}{2}}(M_1^2, t, q^2)} \log \frac{t_1^+ - m_b^2}{t_1^- - m_b^2}, \quad (\text{B.23})$$

where

$$t_1^\mp = t - \frac{M_1^2 - M^2}{2M_1^2} \left[M_1^2 + t - q^2 \pm \lambda^{\frac{1}{2}}(M_1^2, t, q^2) \right] \quad (\text{B.24})$$

$$t^\mp = m_b^2 - \frac{s + Q^2}{2s} \left[s + m_b^2 - M_1^2 \pm \lambda^{\frac{1}{2}}(s, m_b^2, M_1^2) \right], \quad (\text{B.25})$$

and we have omitted an overall proportionality constant which takes into account, among other factors, the result of azimuthal integrations. The collinear singularity occurs at the upper bound of integration, t^+ , which vanishes as $m_b \rightarrow 0$, as can be seen expanding t^\pm Eq. (B.25) in powers of m_b^2 to the first non-trivial order:

$$t^- = -\frac{(s + Q^2)(s - M_1^2)}{s} + O(m_b^2) \quad (\text{B.26})$$

$$t^+ = -m_b^2 \frac{M_1^2 + Q^2}{s - M_1^2} + O(m_b^4). \quad (\text{B.27})$$

We now note that both $\lambda^{-1/2}(M^2, t, q^2)$ and t_1^- Eq. (B.24) are regular in $t = t^+ \rightarrow 0$, and can therefore be computed at $t = t^+$. Indeed

$$t_1^- = -\frac{(M_1^2 - M^2)(M_1^2 + Q^2)}{M_1^2} + O(t) \quad (\text{B.28})$$

$$t_1^+ = t \frac{M^2 + Q^2}{M_1^2 + Q^2} + O(t^2). \quad (\text{B.29})$$

In order to set an upper bound for the most singular contribution to σ^{coll} , Eq. (B.23), we neglect the $\mathcal{O}(t)$ and $\mathcal{O}(t^2)$ contributions in Eqs. (B.28)-(B.29), and note that the limits of integration in t_1 are bound by

$$t_1^- \geq -\frac{(s - M^2)(s + Q^2)}{s} \quad (\text{B.30})$$

$$t_1^+ \leq t^+ \frac{M^2 + Q^2}{M_1^2 + Q^2} = -m_b^2 \frac{M^2 + Q^2}{s - M_1^2} \leq -m_b^2 \frac{M^2 + Q^2}{s - M^2}. \quad (\text{B.31})$$

The first inequality is a consequence of the fact that t_1^- is an increasing function of M_1^2 , and $M_1^2 \leq s$. The second inequality follows from $t \leq t^+$ and $M_1^2 \geq M^2$. In so doing, the integrations in t_1 and t become independent. The integration in t_1 yields

$$\log \frac{t_1^-}{t_1^+ - m_b^2} \leq \log \frac{(s - M^2)^2}{sm_b^2} = \log \frac{\mathcal{Q}^2(z)}{m_b^2}. \quad (\text{B.32})$$

The integration in t , up to less singular terms, gives rise to a logarithm which is also bounded by $\log \mathcal{Q}^2(z)/m_b^2$:

$$\log \frac{t^-}{t^+ - m_b^2} = \log \frac{(s - M_1^2)^2}{sm_b^2} \leq \log \frac{(s - M^2)^2}{sm_b^2} = \log \frac{\mathcal{Q}^2(z)}{m_b^2} \quad (\text{B.33})$$

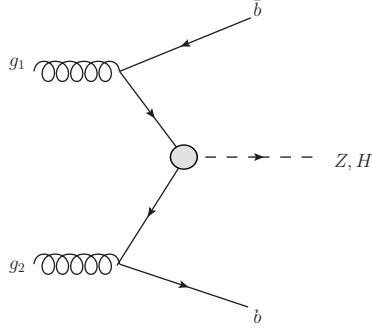


Figure 16. $gg \rightarrow Z/Hbb$ production.

since $M_1^2 \geq M^2$. Thus,

$$\sigma^{\text{coll}} \leq \int_{M^2}^{(\sqrt{s}-m_b)^2} \frac{dM_1^2}{M_1^2 + Q^2} \log^2 \frac{Q^2(z)}{m_b^2}. \quad (\text{B.34})$$

This proves that the argument of the collinear logarithms is bounded from above by $\frac{Q^2(z)}{m_b^2}$ even in presence of one extra emission. The proof can be easily extended to the case of n extra gluon emissions, just noting that the integrations over M_j^2 in Eq. B.21 can be disentangled by using M_n^2 as the upper limit of integration for all of them, neglecting t_j in the $\lambda^{\frac{1}{2}}(M_j^2, t_k, q^2)$ denominators, and then recursively building lower and upper bounds to the t_j^\mp limits.

The above proof can also be used with minor modifications to show that $\frac{Q^2(z)}{m_b^2}$ are universal kinematic terms associated to the collinear logs in processes that can be described via b -PDF for both initial legs, such as Hbb and Zbb production displayed in figure 16.

In this case one can write:

$$\sigma_{\text{coll}} \propto \int_{(m_b+M)^2}^{(\sqrt{s}-m_b)^2} \frac{ds_1}{s_1} \int_{t_2^-}^{t_2^+} \frac{1}{t_2 - m_b^2} dt_2 \int_{t_1^-}^{t_1^+} \frac{1}{t_1 - m_b^2} dt_1 \quad (\text{B.35})$$

with

$$s_1 = (p_{\bar{b}} + p_M)^2 \quad (\text{B.36})$$

$$t_1 = (p_1 - p_{\bar{b}})^2 \quad (\text{B.37})$$

$$t_2 = (p_2 - p_b)^2 \quad (\text{B.38})$$

$$t_1^\pm = m_b^2 - \frac{1}{2} \frac{s_1 - t_2}{s_1} \left[(s_1 - M^2 + m_b^2) \pm \lambda^{\frac{1}{2}}(s_1, M^2, m_b^2) \right] \quad (\text{B.39})$$

$$t_2^\pm = m_b^2 - \frac{1}{2} \left[s - s_1 + m_b^2 \pm \lambda^{\frac{1}{2}}(s, m_b^2, s_1) \right] \quad (\text{B.40})$$

Integration over t_1 directly leads to

$$\log \frac{t_1^- - m_b^2}{t_1^+ - m_b^2} \simeq \log \frac{(s_1 - M^2)^2}{s_1 m_b^2} \quad (\text{B.41})$$

while integration over t_2 gives

$$\log \frac{t_2^- - m_b^2}{t_2^+ - m_b^2} \simeq \log \frac{(s - s_1)^2}{s m_b^2}, \quad (\text{B.42})$$

leading to

$$\sigma_{\text{coll}} \propto \int_{(m_b+M)^2}^{(\sqrt{s}-m_b)^2} \frac{ds_1}{s_1} \log \frac{(s_1 - M^2)^2}{s_1 m_b^2} \log \frac{(s - s_1)^2}{s m_b^2} \quad (\text{B.43})$$

It is easy to see that the $s_1 \sim (\sqrt{s} - m_b)^2$ and $s_1 \sim (m_b + M)^2$ integration regions each give rise to single logs of the form $\log \frac{Q^2(z)}{m_b^2}$. The single logs correspond to the case where only one of the two b 's is collinear to the initial state while the other takes part to the genuine hard scattering (in the 5F language this configuration is described by $gb \rightarrow bh, bZ$). The double log (i.e., the dominant contribution that in the 5F approach leads to the leading order process $bb \rightarrow Z, h$) is obtained from the intermediate region of integration for s_1 , where $s_1 \simeq s_2$ and $s \gg s_1$ and $s_1 \gg M^2$, a region that is always kinematically accessible due to the identity

$$s = s_{bb} - s_1 - s_2 + m_b^2 + m_b^2 + M^2. \quad (\text{B.44})$$

In such a region

$$\log \frac{(s_1 - M^2)^2}{s_1 m_b^2} \log \frac{(s - s_1)^2}{s m_b^2} \simeq \log^2 \frac{Q^2(z)}{m_b^2}. \quad (\text{B.45})$$

C Explicit NLO expression for \tilde{b}

The coefficients $a_{j,b}^{(p)}$ (with $j = \Sigma, g$ and $p = 1, 2$), up to constant terms (that we set to zero in order to fulfil the boundary conditions $\tilde{b}(x, m_b^2) = 0$) are given by [49]

$$a_{g,b}^{(1)} \left(z, \frac{\mu^2}{m_b^2} \right) = 2 P_{qg}(z) \log \frac{\mu^2}{m_b^2} \quad (\text{C.1})$$

$$\begin{aligned}
a_{g,b}^{(2)}\left(z, \frac{\mu^2}{m_b^2}\right) = & \left\{ C_{FT_R} \left[8P_{qg}(z) \log(1-z) - (2-4z+8z^2) \log z - (1-4z) \right. \right. \\
& - C_{AT_R} \left[8P_{qg}(z) \log(1-z) + (4+16z) \log z + \frac{8}{3z} + 2 + 16z - \frac{62}{3}z^2 \right] \\
& \left. \left. + T_R^2 \left[-\frac{8}{3}(z^2 + (1-z)^2) \right] \right\} \log^2 \frac{\mu^2}{m_b^2} \\
& - \left\{ C_{FT_R} \left[8P_{qg}(z) [2 \log z \log(1-z) - \log^2(1-z) + 2\zeta(2)] \right. \right. \\
& \quad - (2-4z+8z^2) \log^2 z - 16z(1-z) \log(1-z) \\
& \quad \left. \left. - (6-8z+16z^2) \log z - 28 + 58z - 40z^2 \right] \right. \\
& \left. + C_{AT_R} \left[(8+16z+16z^2) [\text{Li}_2(-z) + \log z \log(1+z)] + 8P_{qg}(z) \log^2(1-z) \right. \right. \\
& \quad \left. \left. + (4+8z) \log^2 z + 16z\zeta(2) + 16z(1-z) \log(1-z) - \left(4+32z + \frac{176}{3}z^2 \right) \log z \right. \right. \\
& \quad \left. \left. - \frac{80}{9z} + 8 - 100z + \frac{872}{9}z^2 \right] \right\} \log \frac{\mu^2}{m_b^2}, \tag{C.2}
\end{aligned}$$

for the gluon initiated splitting and by

$$\begin{aligned}
a_{\Sigma,b}^{(2)}\left(z, \frac{\mu^2}{m_b^2}\right) = & \left\{ C_{FT_R} \left[-4(1+z) \log z - \frac{8}{3z} - 2 + 2z + \frac{8}{3}z^2 \right] \right\} \log^2 \frac{\mu^2}{m_b^2} \\
& + \left\{ C_{FT_R} \left[-4(1+z) \log^2 z + \left(4 + 20z + \frac{32}{3}z^2 \right) \log z + \frac{80}{9z} - 8 + 24z - \frac{224}{9}z^2 \right] \right\} \log \frac{\mu^2}{m_b^2}, \tag{C.3}
\end{aligned}$$

for the quark-initiated splitting. In the above expression we used the Altarelli-Parisi splitting function P_{qg} defined as

$$P_{qg}(z) = T_R [z^2 + (1-z)^2] \quad T_R = \frac{1}{2}. \tag{C.4}$$

References

- [1] P. Nason, S. Dawson, and R. Ellis, *The One Particle Inclusive Differential Cross-Section for Heavy Quark Production in Hadronic Collisions*, *Nucl.Phys.* **B327** (1989) 49–92.
- [2] M. L. Mangano, P. Nason, and G. Ridolfi, *Heavy quark correlations in hadron collisions at next-to-leading order*, *Nucl. Phys.* **B373** (1992) 295–345.
- [3] N. Greiner, A. Guffanti, T. Reiter, and J. Reuter, *NLO QCD corrections to the production of two bottom-antibottom pairs at the LHC*, *Phys. Rev. Lett.* **107** (2011) 102002, [[arXiv:1105.3624](#)].
- [4] G. Bevilacqua, M. Czakon, C. G. Papadopoulos, R. Pittau, and M. Worek, *Assault on the NLO Wishlist: pp → tt bb*, *JHEP* **09** (2009) 109, [[arXiv:0907.4723](#)].
- [5] A. Bredenstein, A. Denner, S. Dittmaier, and S. Pozzorini, *NLO QCD corrections to top anti-top bottom anti-bottom production at the LHC: 2. full hadronic results*, *JHEP* **03** (2010) 021, [[arXiv:1001.4006](#)].

- [6] J. M. Campbell, R. Frederix, F. Maltoni, and F. Tramontano, *Next-to-Leading-Order Predictions for t -Channel Single-Top Production at Hadron Colliders*, *Phys. Rev. Lett.* **102** (2009) 182003, [[arXiv:0903.0005](#)].
- [7] S. Dittmaier, M. Kramer, M. Spira, and M. Walser, *Charged-Higgs-boson production at the LHC: NLO supersymmetric QCD corrections*, *Phys.Rev.* **D83** (2011) 055005, [[arXiv:0906.2648](#)].
- [8] S. Dawson, C. B. Jackson, L. Reina, and D. Wackerth, *Exclusive Higgs boson production with bottom quarks at hadron colliders*, *Phys. Rev.* **D69** (2004) 074027, [[hep-ph/0311067](#)].
- [9] S. Dittmaier, M. Kramer, Michael, and M. Spira, *Higgs radiation off bottom quarks at the Tevatron and the CERN LHC*, *Phys.Rev.* **D70** (2004) 074010, [[hep-ph/0309204](#)].
- [10] S. Dawson, C. B. Jackson, L. Reina, and D. Wackerth, *Higgs boson production with one bottom quark jet at hadron colliders*, *Phys. Rev. Lett.* **94** (2005) 031802, [[hep-ph/0408077](#)].
- [11] S. Dawson, C. B. Jackson, L. Reina, and D. Wackerth, *Higgs boson production with bottom quarks at hadron colliders*, *Int. J. Mod. Phys.* **A20** (2005) 3353–3355, [[hep-ph/0409345](#)].
- [12] R. Ellis and S. Veseli, *Strong radiative corrections to $W b$ anti- b production in p anti- p collisions*, *Phys.Rev.* **D60** (1999) 011501, [[hep-ph/9810489](#)].
- [13] J. M. Campbell and R. K. Ellis, *Radiative corrections to $Z b$ anti- b production*, *Phys. Rev.* **D62** (2000) 114012, [[hep-ph/0006304](#)].
- [14] F. Febres Cordero, L. Reina, and D. Wackerth, *NLO QCD corrections to W - b - b bar and Z - b - b bar production*, *PoS RADCOR2007* (2007) 012, [[arXiv:0801.2374](#)].
- [15] F. Febres Cordero, L. Reina, and D. Wackerth, *NLO QCD corrections to $Z b \bar{b}$ production with massive bottom quarks at the Fermilab Tevatron*, *Phys. Rev.* **D78** (2008) 074014, [[arXiv:0806.0808](#)].
- [16] F. Febres Cordero, L. Reina, and D. Wackerth, *W - and Z -boson production with a massive bottom-quark pair at the Large Hadron Collider*, *Phys. Rev.* **D80** (2009) 034015, [[arXiv:0906.1923](#)].
- [17] S. Badger, J. M. Campbell, and R. K. Ellis, *QCD corrections to the hadronic production of a heavy quark pair and a W -boson including decay correlations*, *JHEP* **03** (2011) 027, [[arXiv:1011.6647](#)].
- [18] R. Frederix *et. al.*, *W and Z/γ^* boson production in association with a bottom-antibottom pair*, *JHEP* **09** (2011) 061, [[arXiv:1106.6019](#)].
- [19] S. Frixione and M. L. Mangano, *Heavy quark jets in hadronic collisions*, *Nucl. Phys.* **B483** (1997) 321–338, [[hep-ph/9605270](#)].
- [20] A. Banfi, G. P. Salam, and G. Zanderighi, *Accurate QCD predictions for heavy-quark jets at the Tevatron and LHC*, *JHEP* **0707** (2007) 026, [[arXiv:0704.2999](#)].
- [21] B. W. Harris, E. Laenen, L. Phaf, Z. Sullivan, and S. Weinzierl, *The Fully differential single top quark cross-section in next to leading order QCD*, *Phys. Rev.* **D66** (2002) 054024, [[hep-ph/0207055](#)].
- [22] N. Kidonakis, *Single top production at the Tevatron: Threshold resummation and finite-order soft gluon corrections*, *Phys. Rev.* **D74** (2006) 114012, [[hep-ph/0609287](#)].
- [23] J. M. Campbell, R. K. Ellis, and F. Tramontano, *Single top production and decay at next-to-leading order*, *Phys. Rev.* **D70** (2004) 094012, [[hep-ph/0408158](#)].

- [24] J. M. Campbell and F. Tramontano, *Next-to-leading order corrections to $W t$ production and decay*, *Nucl. Phys.* **B726** (2005) 109–130, [[hep-ph/0506289](#)].
- [25] Q.-H. Cao, R. Schwienhorst, and C. P. Yuan, *Next-to-leading order corrections to single top quark production and decay at Tevatron. 1. s -channel process*, *Phys. Rev.* **D71** (2005) 054023, [[hep-ph/0409040](#)].
- [26] Q.-H. Cao, R. Schwienhorst, J. A. Benitez, R. Brock, and C. P. Yuan, *Next-to-leading order corrections to single top quark production and decay at the Tevatron: 2. t -channel process*, *Phys. Rev.* **D72** (2005) 094027, [[hep-ph/0504230](#)].
- [27] S. Frixione, E. Laenen, P. Motylinski, B. R. Webber, and C. D. White, *Single-top hadroproduction in association with a W boson*, *JHEP* **07** (2008) 029, [[arXiv:0805.3067](#)].
- [28] T. Plehn, *Charged Higgs boson production in bottom gluon fusion*, *Phys. Rev.* **D67** (2003) 014018, [[hep-ph/0206121](#)].
- [29] C. Weydert *et. al.*, *Charged Higgs boson production in association with a top quark in MC@NLO*, *Eur. Phys. J.* **C67** (2010) 617–636, [[arXiv:0912.3430](#)].
- [30] F. Maltoni, Z. Sullivan, and S. Willenbrock, *Higgs-boson production via bottom-quark fusion*, *Phys.Rev.* **D67** (2003) 093005, [[hep-ph/0301033](#)].
- [31] J. M. Campbell, R. Ellis, F. Maltoni, and S. Willenbrock, *Higgs-Boson production in association with a single bottom quark*, *Phys.Rev.* **D67** (2003) 095002, [[hep-ph/0204093](#)].
- [32] J. M. Campbell *et. al.*, *Associated Production of a W Boson and One b Jet*, *Phys. Rev.* **D79** (2009) 034023, [[arXiv:0809.3003](#)].
- [33] J. M. Campbell, R. K. Ellis, F. Maltoni, and S. Willenbrock, *Associated production of a Z Boson and a single heavy quark jet*, *Phys. Rev.* **D69** (2004) 074021, [[hep-ph/0312024](#)].
- [34] J. M. Campbell, R. K. Ellis, F. Maltoni, and S. Willenbrock, *Production of a Z boson and two jets with one heavy- quark tag*, *Phys. Rev.* **D73** (2006) 054007, [[hep-ph/0510362](#)].
- [35] J. M. Campbell, R. K. Ellis, F. Maltoni, and S. Willenbrock, *Production of a W boson and two jets with one b^- quark tag*, *Phys. Rev.* **D75** (2007) 054015, [[hep-ph/0611348](#)].
- [36] R. V. Harlander and W. B. Kilgore, *Higgs boson production in bottom quark fusion at next-to-next-to leading order*, *Phys.Rev.* **D68** (2003) 013001, [[hep-ph/0304035](#)].
- [37] F. Maltoni, T. McElmurry, and S. Willenbrock, *Inclusive production of a Higgs or Z boson in association with heavy quarks*, *Phys. Rev.* **D72** (2005) 074024, [[hep-ph/0505014](#)].
- [38] S. Dawson, C. Kao, Y. Wang, and P. Williams, *QCD Corrections to Higgs Pair Production in Bottom Quark Fusion*, *Phys.Rev.* **D75** (2007) 013007, [[hep-ph/0610284](#)].
- [39] M. Kramer, 1, *Associated Higgs production with bottom quarks at hadron colliders*, *Nucl. Phys. Proc. Suppl.* **135** (2004) 66–70, [[hep-ph/0407080](#)].
- [40] **LHeC Study Group** Collaboration, M. Klein, *The LHeC conceptual design*, *PoS ICHEP2010* (2010) 520.
- [41] S. Frixione and B. R. Webber, *Matching NLO QCD computations and parton shower simulations*, *JHEP* **06** (2002) 029, [[hep-ph/0204244](#)].
- [42] P. Nason, *A New Method for Combining NLO QCD with Shower Monte Carlo Algorithms*, *JHEP* **0411** (2004) 040, [[hep-ph/0409146](#)].
- [43] J. C. Collins, F. Wilczek, and A. Zee, *Low-Energy Manifestations of Heavy Particles:*

- Application to the Neutral Current*, *Phys. Rev.* **D18** (1978) 242.
- [44] M. A. G. Aivazis, J. C. Collins, F. I. Olness, and W.-K. Tung, *Leptoproduction of heavy quarks. 2. A Unified QCD formulation of charged and neutral current processes from fixed target to collider energies*, *Phys. Rev.* **D50** (1994) 3102–3118, [[hep-ph/9312319](#)].
- [45] M. Kramer, F. I. Olness, and D. E. Soper, *Treatment of heavy quarks in deeply inelastic scattering*, *Phys. Rev.* **D62** (2000) 096007, [[hep-ph/0003035](#)].
- [46] W.-K. Tung, S. Kretzer, and C. Schmidt, *Open heavy flavor production in QCD: Conceptual framework and implementation issues*, *J. Phys.* **G28** (2002) 983–996, [[hep-ph/0110247](#)].
- [47] R. S. Thorne and R. G. Roberts, *An ordered analysis of heavy flavour production in deep inelastic scattering*, *Phys. Rev.* **D57** (1998) 6871–6898, [[hep-ph/9709442](#)].
- [48] R. Thorne, *A Variable-flavor number scheme for NNLO*, *Phys.Rev.* **D73** (2006) 054019, [[hep-ph/0601245](#)].
- [49] M. Buza, Y. Matiounine, J. Smith, and W. L. van Neerven, *Charm electroproduction viewed in the variable-flavour number scheme versus fixed-order perturbation theory*, *Eur. Phys. J.* **C1** (1998) 301–320, [[hep-ph/9612398](#)].
- [50] M. Cacciari, M. Greco, and P. Nason, *The $p(T)$ spectrum in heavy-flavour hadroproduction*, *JHEP* **05** (1998) 007, [[hep-ph/9803400](#)].
- [51] S. Forte, E. Laenen, P. Nason, and J. Rojo, *Heavy quarks in deep-inelastic scattering*, *Nucl. Phys.* **B834** (2010) 116–162, [[arXiv:1001.2312](#)].
- [52] R. D. Ball *et. al.*, *Impact of Heavy Quark Masses on Parton Distributions and LHC Phenomenology*, [arXiv:1101.1300](#).
- [53] **The NNPDF Collaboration** Collaboration, R. D. Ball *et. al.*, *Unbiased global determination of parton distributions and their uncertainties at NNLO and at LO*, *Nucl.Phys.* **B855** (2012) 153–221, [[arXiv:1107.2652](#)]. 80 pages, 51 figures. Final version, to be published in Nuclear Physics B.
- [54] A. D. Martin, W. J. Stirling, R. S. Thorne, and G. Watt, *Parton distributions for the LHC*, *Eur. Phys. J.* **C63** (2009) 189–285, [[arXiv:0901.0002](#)].
- [55] H.-L. Lai, M. Guzzi, J. Huston, Z. Li, P. M. Nadolsky, *et. al.*, *New parton distributions for collider physics*, *Phys.Rev.* **D82** (2010) 074024, [[arXiv:1007.2241](#)].
- [56] **H1 and ZEUS Collaboration** Collaboration, F. Aaron *et. al.*, *Combined Measurement and QCD Analysis of the Inclusive e^+p Scattering Cross Sections at HERA*, *JHEP* **1001** (2010) 109, [[arXiv:0911.0884](#)]. 61 pages, 21 figures.
- [57] S. Alekhin, J. Blumlein, and S. Moch, *Parton distribution functions and benchmark cross sections at NNLO*, [arXiv:1202.2281](#).
- [58] P. Jimenez-Delgado and E. Reya, *Variable Flavor Number Parton Distributions and Weak Gauge and Higgs Boson Production at Hadron Colliders at NNLO of QCD*, *Phys.Rev.* **D80** (2009) 114011, [[arXiv:0909.1711](#)]. 28 pages, 3 tables, 6 figures.
- [59] **SM and NLO Multileg Working Group** Collaboration, J. R. Andersen *et. al.*, *The SM and NLO multileg working group: Summary report*, [arXiv:1003.1241](#).
- [60] A. Chuvakin and J. Smith, *Evolution program for parton densities with perturbative heavy flavor boundary conditions*, *Comput.Phys.Commun.* **143** (2002) 257–286, [[hep-ph/0103177](#)].

- [61] I. Bierenbaum, J. Blumlein, and S. Klein, *The Gluonic Operator Matrix Elements at $O(\alpha_s^2)$ for DIS Heavy Flavor Production*, *Phys.Lett.* **B672** (2009) 401–406, [[arXiv:0901.0669](#)].
- [62] M. Buza, Y. Matiounine, J. Smith, R. Migneron, and W. van Neerven, *Heavy quark coefficient functions at asymptotic values $Q^2 \gg m^2$* , *Nucl.Phys.* **B472** (1996) 611–658, [[hep-ph/9601302](#)].
- [63] I. Bierenbaum, J. Blumlein, and S. Klein, *Two-Loop Massive Operator Matrix Elements and Unpolarized Heavy Flavor Production at Asymptotic Values $Q^2 \gg m^2$* , *Nucl.Phys.* **B780** (2007) 40–75, [[hep-ph/0703285](#)]. Dedicated to the Memory of W.L. van Neerven.
- [64] I. Bierenbaum, J. Blumlein, S. Klein, and C. Schneider, *Two-Loop Massive Operator Matrix Elements for Unpolarized Heavy Flavor Production to $O(\epsilon)$* , *Nucl.Phys.* **B803** (2008) 1–41, [[arXiv:0803.0273](#)].
- [65] I. Bierenbaum, J. Blumlein, and S. Klein, *Mellin Moments of the $O(\alpha_s^3)$ Heavy Flavor Contributions to unpolarized Deep-Inelastic Scattering at $Q^2 \gg m^2$ and Anomalous Dimensions*, *Nucl. Phys.* **B820** (2009) 417–482, [[arXiv:0904.3563](#)].
- [66] S. Alekhin, J. Blumlein, S. Klein, and S. Moch, *The 3, 4, and 5-flavor NNLO Parton from Deep-Inelastic-Scattering Data and at Hadron Colliders*, *Phys.Rev.* **D81** (2010) 014032, [[arXiv:0908.2766](#)]. 33 pages, 14 figures, Journal version.
- [67] J. M. Campbell, R. Frederix, F. Maltoni, and F. Tramontano, *NLO predictions for t -channel production of single top and fourth generation quarks at hadron colliders*, *JHEP* **10** (2009) 042, [[arXiv:0907.3933](#)].
- [68] J. M. Campbell *et. al.*, *Higgs boson production in association with bottom quarks*, [[hep-ph/0405302](#)].
- [69] F. I. Olness and S. T. Riemersma, *Leptoproduction of heavy quarks in the fixed and variable flavor schemes*, *Phys.Rev.* **D51** (1995) 4746–4755, [[hep-ph/9409208](#)].
- [70] W. L. van Neerven, *Production of heavy quarks in deep inelastic lepton hadron scattering*, [[hep-ph/0107193](#)].
- [71] W. K. Tung *et. al.*, *Heavy quark mass effects in deep inelastic scattering and global QCD analysis*, *JHEP* **02** (2007) 053, [[hep-ph/0611254](#)].
- [72] F. Olness and I. Schienbein, *Heavy Quarks: Lessons Learned from HERA and Tevatron*, *Nucl. Phys. Proc. Suppl.* **191** (2009) 44–53, [[arXiv:0812.3371](#)].
- [73] A. D. Martin, W. J. Stirling, R. S. Thorne, and G. Watt, *Heavy-quark mass dependence in global PDF analyses and 3- and 4-flavour parton distributions*, *Eur. Phys. J.* **C70** (2010) 51–72, [[arXiv:1007.2624](#)].
- [74] R. S. Thorne and W. K. Tung, *PQCD Formulations with Heavy Quark Masses and Global Analysis*, [[arXiv:0809.0714](#)].
- [75] R. Thorne, *The Effect of Changes of Variable Flavour Number Scheme on PDFs and Predicted Cross Sections*, [[arXiv:1201.6180](#)].
- [76] **H1 Collaboration** Collaboration, F. Aaron *et. al.*, *Measurement of the Charm and Beauty Structure Functions using the H1 Vertex Detector at HERA*, *Eur.Phys.J.* **C65** (2010) 89–109, [[arXiv:0907.2643](#)]. 40 pages, 4 tables, 18 figures.
- [77] **H1 Collaboration**, F. D. Aaron *et. al.*, *Measurement of the D^* Meson Production Cross Section and F_2^{ccbar} , at High Q^2 , in ep Scattering at HERA*, *Phys. Lett.* **B686** (2010)

- 91–100, [[arXiv:0911.3989](#)].
- [78] **H1** Collaboration, F. D. Aaron *et. al.*, *Measurement of Charm and Beauty Jets in Deep Inelastic Scattering at HERA*, *Eur. Phys. J.* **C71** (2011) 1509, [[arXiv:1008.1731](#)].
- [79] **H1** Collaboration, F. D. Aaron *et. al.*, *Measurement of D^* Meson Production and Determination of F_2^{ccbar} at low Q^2 in Deep-Inelastic Scattering at HERA*, *Eur. Phys. J.* **C71** (2011) 1769, [[arXiv:1106.1028](#)].
- [80] **ZEUS Collaboration** Collaboration, S. Chekanov *et. al.*, *Measurement of beauty production in deep inelastic scattering at HERA*, *Phys.Lett.* **B599** (2004) 173–189, [[hep-ex/0405069](#)].
- [81] **ZEUS** Collaboration, S. Chekanov *et. al.*, *Measurement of charm and beauty production in deep inelastic ep scattering from decays into muons at HERA*, *Eur. Phys. J.* **C65** (2010) 65–79, [[arXiv:0904.3487](#)].
- [82] **ZEUS** Collaboration, H. Abramowicz *et. al.*, *Measurement of beauty production in deep inelastic scattering at HERA using decays into electrons*, *Eur. Phys. J.* **C71** (2011) 1573, [[arXiv:1101.3692](#)].
- [83] J. Smith and B. W. Harris, *Heavy-quark correlations in deep inelastic scattering*, *Nucl. Phys. Proc. Suppl.* **51C** (1996) 188–194, [[hep-ph/9605358](#)].
- [84] E. Laenen, S. Riemersma, J. Smith, and W. L. van Neerven, *Complete $O(\alpha_s)$ corrections to heavy flavor structure functions in electroproduction*, *Nucl. Phys.* **B392** (1993) 162–228.
- [85] S. Forte and G. Ridolfi, *Renormalization group approach to soft gluon resummation*, *Nucl.Phys.* **B650** (2003) 229–270, [[hep-ph/0209154](#)].
- [86] S. S. Willenbrock and D. A. Dicus, *Production of Heavy Quarks from W Gluon Fusion*, *Phys.Rev.* **D34** (1986) 155.
- [87] C. Yuan, *A New Method to Detect a Heavy Top Quark at the Tevatron*, *Phys.Rev.* **D41** (1990) 42.
- [88] R. Ellis and S. J. Parke, *Top quark production by W gluon fusion*, *Phys.Rev.* **D46** (1992) 3785–3788.
- [89] G. Bordes and B. van Eijk, *Calculating QCD corrections to single top production in hadronic interactions*, *Nucl.Phys.* **B435** (1995) 23–58.
- [90] T. Stelzer, Z. Sullivan, and S. Willenbrock, *Single top quark production via W - gluon fusion at next-to-leading order*, *Phys.Rev.* **D56** (1997) 5919–5927, [[hep-ph/9705398](#)].
- [91] **CDF** Collaboration, T. Aaltonen *et. al.*, *First measurement of the production of a W boson in association with a single charm quark in p anti- p collisions at $s^{**}(1/2) = 1.96$ -TeV*, *Phys. Rev. Lett.* **100** (2008) 091803, [[arXiv:0711.2901](#)].
- [92] **CMS Collaboration** Collaboration, *Study of associated charm production in W final states at $\sqrt{s} = 7$ TeV*, CMS-PAS-EWK-11-013.
- [93] F. I. Olness and W.-K. Tung, *When Is a Heavy Quark Not a Parton? Charged Higgs Production and Heavy Quark Mass Effects in the QCD Based Parton Model*, *Nucl.Phys.* **B308** (1988) 813.
- [94] J. M. Campbell, R. Ellis, and D. L. Rainwater, *Next-to-leading order QCD predictions for $W + 2$ jet and $Z + 2$ jet production at the CERN LHC*, *Phys.Rev.* **D68** (2003) 094021, [[hep-ph/0308195](#)].

- [95] E. Boos and T. Plehn, *Higgs boson production induced by bottom quarks*, *Phys.Rev.* **D69** (2004) 094005, [[hep-ph/0304034](#)].
- [96] F. Maltoni, T. McElmurry, R. Putman, and S. Willenbrock, *Choosing the factorization scale in perturbative QCD*, [hep-ph/0703156](#).
- [97] R. Harlander, M. Kramer, and M. Schumacher, *Bottom-quark associated Higgs-boson production: reconciling the four- and five-flavour scheme approach*, [arXiv:1112.3478](#).
- [98] B. W. Harris and J. Smith, *Heavy quark correlations in deep inelastic electroproduction*, *Nucl. Phys.* **B452** (1995) 109–160, [[hep-ph/9503484](#)].
- [99] E. Byckling, K. Kajantie, *Particle Kinematics*. Wiley, 1973.